AN INFRARED MONOCHROMATOR SYSTEM AND PHOTOCONDUCTIVITY IN SOME III-V ALLOYS

by

Alan E. Taylor

Submitted in partial fulfillment
of the requirements for the degree of
Master of Science

Department of Physics,
Faculty of Science and Engineering,
University of Ottawa,
OTTAWA, Canada

1970

ACKNOWLEDGEMENTS

The author wishes to thank Dr. E. Fortin for suggesting the problem and for his supervision throughout the course of the research. Thanks are due as well to Mr. C. N. Goodchild and the Technicians for the construction of the cryostat and all the accessory hardware forming the monochromator system; to Mr. J. N. Cairns of the Optics Shop of the National Research Council for the mirrors; to the other students in the department, with whom useful discussions were often held; and finally to Miss Diane Dubé and Miss Loretta Sawyer for typing the thesis. The author is grateful to the Province of Ontario for financial support in the form of a Graduate Fellowship.

ABSTRACT

A complete monochromatic system and low signal detection electronics useful for photoconductive studies and other experiments in the infrared are described. This system was used to recover photosignals as low as 2×10^{-8} volts from low resistance samples. Photoconductive properties of GaAs-InAs and GaAs-GaSb alloys with carrier concentrations in the range 10^{16} to 10^{18} cm^{-3} were investigated at $300^{o}K$, $210^{o}K$ and $100^{o}K$. These alloys were used 'as grown' with no deliberate attempt to reduce their relatively high carrier concentrations by introducing compensating impurities. The photoresponse curves of the samples were spread smoothly across the alloy ranges. Bandgaps were determined from the spectral sensitivity curves, and a smooth variation was obtained. Previous work done by other investigators on GaAs-InAs at room temperature showed close agreement with these bandgap values. For GaAs-GaSb, the complete alloy range of material is not yet available; however, bandgap values obtained near the ends of the range suggest a minimum in a smooth variation with composition at all three temperatures. Finally, an assessment of these alloys as detectors is made. The room temperature detectivity of the samples was between 5×10^{4} and 8×10^{6} $cm(Hz)^{\frac{1}{2}}$ $(watt)^{-1}$ for wavelengths of the peak responses.

TABLE OF CONTENTS

LIST OF ILLUSTRATIONS

LIST OF TABLES

CHAPTER 1

INTRODUCTION

1.1 Photoconductivity

As the name implies, photoconductivity is the effect whereby electrical conductivity of a solid changes under the action of light. This effect, first observed by Smith[1] in 1873 on selenium, has become increasingly prominent in recent years. There are several reasons for this.

First, photoconductivity is used as a basic research technique to complement other optical methods of studying materials. Second, improved manufacturing techniques have made feasible the production of photoconductive devices and detectors using a wide range of materials. The availability and study of many semiconductors has permitted the manufacture of infrared quantum detectors with detectivity and response speed surpassing that of the older thermal detectors.

1.2 Materials

The earliest semiconductors to be studied were silicon and germanium; their impressive electrical properties and application possibilities prompted a search for other materials, among them being the wide selection of semiconducting compounds. The compounds of groups III and V of the periodic table were among the first to be investigated. By the early 1950's, the semiconducting materials which had been studied provided a discrete range of physical parameters.

A natural extension of these investigations was the attempt to alloy various semiconductor materials in order to obtain a continuous range of these parameters. Considerable success has been achieved in studies of the III-V alloys in this laboratory and elsewhere. In photoconductivity, semiconductor alloys present the possibility of making detectors with thresholds anywhere over a range of infrared wavelengths.

1.3 Summary of Project

The present work on photoconductivity in the III-V alloys was planned to complement the considerable optical and electrical studies undertaken at this University. Little work in photoconductivity has previously been done here.

Elsewhere however, some alloy photoconductivity measurements have been made. Wrobel and Levinstein[2] investigated the systems GaSb-InSb and GaAs-InAs but required compensation with suitable impurities or low temperatures to overcome the high carrier concentrations normally encountered in these alloys. Recent advances in the techniques of low signal detection have permitted photoconductivity measurements to be done on material of comparatively high carrier concentrations and at room temperature. The object of this investigation was to attempt to use the alloy material "as grown", and without any delibrate compensation.

The project was started with the design and set-up of an experimental system that would be useful in this work and future studies in the infrared. Photoconductive response curves were obtained for 12 samples in the GaAs-InAs system, and for 6 samples from the limited alloy material available in the GaAs-GaSb system. For most samples the experiments were done at three temperatures: $300^{o}K$, $210^{o}K$, and $100^{o}K$. The photoresponse curves are presented as a function of mole percent, and the energy bandgaps were calculated from these curves. A smooth variation of bandgap with composition was observed in each system. Values showed good agreement with energy gap values determined by other workers in this laboratory and elsewhere.

Similar experiments were attempted on two other systems. No results were obtained for alloy material in the InAs-InSb system, but limited success was achieved at the GaSb-rich end of GaSb-InSb

The considerable use of some of the compound semiconductors as infrared detectors motivated further investigation of the radiation detecting ability of the corresponding alloy material. Measurements on some of the samples yielded responsivity values from 10^{-3} to 10^{-2} volts $(watt)^{-1}$ and detectivity values in the range from 2×10^{5} to 8×10^{6} $cm(Hz)^{\frac{1}{2}}(watt)^{-1}$. Similar experiments on a Kodak PbSe cell gave values of about 50 volts $(watt)^{-1}$ for responsivity and $4 \times 10^{8} cm(Hz)^{\frac{1}{2}}(watt)^{-1}$ for detectivity.

Before the descriptions of the equipment and the results are presented, theory appropriate for this project will be given. Some basic concepts of band theory as applied to photoconductivity will be given first, followed by a more detailed discussion of the processes involved. Finally, two models describing the general shape of the photoresponse will be given in some mathematical detail.

CHAPTER II

THEORY

II.1 Introduction

Just as electrons in isolated atoms cannot possess any arbitrary energy, the electrons in a crystalline solid cannot have a continuous energy distribution. In the solid, the discrete energy levels of the atom are broadened into bands of energy separated by forbidden zones, and the electrons occupying the bands are not associated with any particular atom. Electrical and optical studies of solids deal with the upper filled, partially filled and nearby higher bands in a way analogous to the study of energy levels in atomic physics. In an insulator, the valence electrons exactly fill the valence bands and conduction will not be possible. A semiconductor is an insulator in which some of the electrons are in the conduction band at thermal equilibrium.

The basic process of photoconductivity is the production of free charge carriers in a semiconductor by optical excitation. In intrinsic material, the electrons are raised from the valence band to the conduction band, where they are free to conduct; the holes left in the valence band contribute to the conductivity as well. In a semiconductor containing

impurity atoms or imperfections in the lattice, there will be energy levels in the forbidden gap. In n-type material, it is possible to excite electrons from a bound state at donor levels into the conduction band. In p-type material, electrons can be excited from the valence band to acceptor centers, leaving mobile holes. In the latter cases, only one type of carrier is produced, and this impurity photoconductivity occurs in addition to the intrinsic response.

Photoconductivity will occur in semiconductors if the exciting radiation is of sufficiently high energy to exceed the energy transition involved. This investigation is concerned principally with intrinsic photoconductivity.

II.2 Preliminary concepts in photoconductivity

Some concepts of the processes involved in photoconductivity will be introduced, before a more detailed theory is presented in following sections. The conductivity of a semiconductor is expressed as

$$\sigma = e(n\mu_n + p\mu_p) \qquad (1\text{-}1)$$

The symbols have the usual significance and are given in the symbol chart, Table I. Absorbed radiation will increase the conductivity because of the Δn electrons raised to the conduction band and the Δp holes created in the valence band.

$$\Delta\sigma = e\,(\Delta n\mu_n + \Delta p\mu_p) \tag{1-2}$$

Generally for semi-insulating semiconductors,

$$\Delta n >> n_o \;;\; \Delta p >> p_o \tag{1-3}$$

$$\Delta\sigma >> \sigma \tag{1-4}$$

In semiconductors with high carrier concentrations, the dark conductivity is much larger than the photo-induced conductivity:

Thus
$$\Delta\sigma << \sigma \tag{1-5}$$

$$\Delta n << n_o \;;\; \Delta p << p_o \tag{1-6}$$

The latter case is the one of interest in the present work.

The processes of carrier creation and subsequent recombination lead to an equilibrium being established. The times that these electrons and holes are free to conduct are called the free lifetimes, τ_n and τ_p, respectively. If the light on the surface creates G electron - hole pairs per second and per unit volume, then the excess equilibrium concentrations are

$$\begin{aligned} \Delta n &= G\tau_n \\ \Delta p &= G\tau_p \\ \Delta\sigma &= Ge(\tau_n\mu_n + \tau_p\mu_p) \end{aligned} \tag{1-7}$$

In material with high carrier concentrations, recombination is predominantly the direct combination of a hole and an electron. This is termed bimolecular recombination. For low carrier concentrations, the main process is the capture of one carrier by an imperfection and subsequent recombination with a free carrier. In the recombination of photoexcited electrons and holes, the excess energy is dissipated by phonons, low energy photons, or by three body collisions.

It is the recombination process which determines the lifetimes of the carriers, and hence the photosensitivity of the material. Surface lifetimes are usually much shorter than the volume lifetimes, because the surface of the sample deviates from the crystalline arrangement of the bulk. In addition, most of the light is absorbed near the surface. This creates a high carrier density in this region and gives a higher probability of bimolecular recombination.

A curve of photoresponse versus wavelength has a characteristic shape: starting with a plateau at shorter wavelengths, rising to a pronounced maximum prior to the absorption edge, and falling exponentially with wavelength through the bandgap at longer wavelengths. A short theory of this response will now be given.

TABLE I

Symbols

n_o, p_o = density of free holes in dark (m^{-3})

n, p = density of free electrons, free holes, (m^{-3})

n, p = density of free electrons, free holes (m^{-3})

μ_n, μ_p = mobilities of free electrons, free holes (m^2 $volt^{-1}$ sec^{-1})

b = μ_n/μ_p = mobility ratio

q = quantum efficiency

α = absorption coefficient (m^{-1})

H = irradiance (watt m^{-2})

ν = frequency of light (Hz)

s = surface recombination velocity (m sec^{-1})

D = Diffusion constant for holes ($m^2 sec^{-1}$)

L = Diffusion length for holes (m)

d = thickness of sample (m)

w = width of sample (m)

F = electric field (volts m^{-1})

T = temperature (^oK)

K = Boltzmann's constant (joules $^oK^{-1}$)

II-3. Photoresponse at wavelengths shorter than the spectral peak

At short wavelengths where the penetration of the light is least, processes occuring near the surface govern the photoresponse. A suitable model for the response in this region is given by Smith[3]. An n-type material is assumed. Although the continuity and transport equations will be given in terms of the excess hole density Δp, similar equations may be developed for the photoelectrons.

The equation of continuity for the holes in the material is given by

$$\frac{\partial p}{\partial t} + \frac{1}{e} \operatorname{div} \vec{J}p = \text{(generation minus recombination rate)} = g - r \qquad (2\text{-}1)$$

where $p = p_0 + \Delta p$

$g = Ge^{-\alpha x}$, the generation rate

$G = \frac{q\alpha H}{h\nu}$, the generation rate of the surface ($x = 0$)

$r = \frac{\Delta p}{\tau_p}$, the recombination rate, where τ_p is the hole lifetime in the bulk

$\vec{J}p$ is the hole current density. It is composed of the drift current density arising from the external field $\vec{F}$ acting on the p holes, and the diffusion of the holes.

$$\vec{J}p = pe\mu_p\vec{F} - eD \operatorname{grad} p \qquad (2\text{-}2)$$

Putting these values into (2-1) gives

$$\frac{\partial p}{\partial t} + p\,\mu_p \operatorname{div} \vec{F} - D \operatorname{div} \operatorname{grad} p = Ge^{-\alpha x} - \frac{\Delta p}{\tau_p} \qquad (2\text{-}3)$$

i) Maxwell's equation gives the divergence of the electric field:

$$\operatorname{div} \vec{F} \sim \Delta p - \Delta n$$

We assume charge neutrality exists throughout the specimen, so

$$\Delta p = \Delta n, \quad \text{and} \quad \operatorname{div} \vec{F} = 0$$

ii) The photodiffusion voltage arising from the different mobilities of holes and electrons is not considered. Moss[21] shows it to be a small effect when the absorption constant is large.

iii) End effects are neglected and p is assumed uniform in y and z (surface coordinates). Thus,

$$\operatorname{div} \operatorname{grad} p. = \frac{\partial^2 p}{\partial x^2} + \frac{\partial^2 p}{\partial y^2} + \frac{\partial^2 p}{\partial z^2} = \frac{\partial^2 p}{\partial X^2} = \frac{\partial^2 \Delta p}{\partial X^2}$$

iv) The sample is assumed thick enough compared with the diffusion length L so that the unilluminated face needn't be considered.

v) Since only the equilibrium photoresponse is studied in this work,

$$\frac{\partial p}{\partial t} = 0$$

With the above substitutions in eq. (2-3), a one dimensional equation results:

$$D \frac{d^2 \Delta p}{dx^2} - \frac{\Delta p}{\tau_p} = -Ge^{-\alpha x} \qquad (2\text{-}4)$$

An appropriate solution is

$$\Delta p = Ae^{-x/L} - \frac{\tau_p G e^{-\alpha x}}{L^2 \alpha^2 - 1} \qquad (2\text{-}5)$$

where A and L are constants. Substituting in eq. (2-4)

$$\left(\frac{DA}{L^2} - \frac{A}{\tau_p}\right) e^{-x/L} + \left(\frac{G - D\tau_p G\alpha^2}{L^2\alpha^2 - 1}\right) e^{-\alpha x} = -Ge^{-\alpha x} \qquad (2\text{-}6)$$

This identity requires the first coefficient to be zero:

$$\left(\frac{DA}{L^2} - \frac{A}{\tau_p}\right) = 0 \; ; \; L = (D\tau_p)^{1/2} \qquad (2\text{-}7)$$

where L is the diffusion length for holes. The coefficient of the second term in eq. (2-6) reduces to -G with this substitution for L.

The constant A is determined by the boundary condition at the surface x = 0. The rate at which carriers are absorbed in the surface region is $s\Delta p$, where s is a convenient parameter called the surface recombination velocity. It is proportional to the average thermal velocity near the surface. (The recombination rate at the surface is proportional to $s\Delta p$).

The diffusion current of the excess carriers in the x direction is proportional to $D \frac{\partial \Delta p}{\partial x}$. Thus a suitable boundary condition is

$$D \frac{\partial \Delta p}{\partial x} = s \Delta p \qquad \text{at } x = 0 \tag{2-8}$$

This condition gives A in terms of s and other constants:

$$A = \frac{G\tau_p}{\alpha^2 L^2 - 1} \quad \frac{\alpha L^2 + s\tau_p}{L + s_p} \tag{2-9}$$

The final expression for the excess carrier density as a function of depth from the illuminated surface is

$$\Delta p(x) = \frac{G\tau_p}{\alpha^2 L^2 - 1} \quad \frac{L^2 + s\tau_p}{L + s\tau_p} \cdot e^{-x/L} - e^{-\alpha x} \tag{2-10}$$

The penetration depth at which the radiation falls off to 1/e is α^{-1}. Thus for a penetration depth much less than the ambipolar diffusion length L, (i.e. $\alpha L >> 1$), the final exponential term disappears more rapidly than the first, and the excess holes penetrate to a much greater depth than the radiation. As $\alpha \to \infty$ (at wavelengths much shorter than the bandgap), the last term approaches zero and the carriers created near the surface penetrate a distance equal to L. This is the surface region where the probability of recombination is high.

The current density is the sum of the hole current density described in eq. (2-2) and the electron current density.

$$\vec{J} = \vec{J}_p + \vec{J}_n$$

$$= e\mu_p \vec{F}(p + bn) + eD(b \text{ grad } n - \text{grad } p)$$

$$= e\mu_p \vec{F}(p_o + bn_o) + e\mu_p \vec{F}(\Delta p + b\Delta n) + eD(b \text{ grad } \Delta n - \text{grad } \Delta p)$$

(2-11)

If $\vec{F}$, the external field, is applied along the y direction, the x and z components of $\vec{J}$ are zero for equilibrium. Since p is uniform in the y direction,

$$\frac{\partial \Delta p}{\partial y} = 0$$

Then the current density which gives rise to the observed current is

$$J_y = e\mu_p F(p_o + bn_o) + e\mu_p F(1 + b)\,\Delta p \qquad (2\text{-}12)$$

The first term is the dark current density, and the second is the photocurrent density.

To find the photocurrent which is observed, we multiply the photocurrent density by the illuminated area W and integrate inwards from the surface x = 0 to x = d. The contribution to this integral over x where d >> L is negligible and we assume d → ∞ for mathematical convenience. Thus the observed photocurrent is

$$i_{pc} = W \int_0^\infty J_y\, dx$$

$$= eF(1 + b)\, {}_pW \int \Delta p\, dx \qquad (2\text{-}13)$$

Substituting for Δp from eq. (2-10) gives

$$i_{pc} = \frac{eq\, wLH\tau_p\mu_p\, (1 + b)F}{h\nu(L + s\tau_p)} \left(1 + \frac{s\tau_p}{L}\right) \cdot \frac{1}{1 + \alpha L} \qquad (2\text{-}14)$$

The photocurrent may be written more simply as

$$i_p = i_p(\infty) \quad 1 + \frac{s\tau_p}{L} \left(\frac{1}{1 + \alpha L}\right) \qquad (2\text{-}15)$$

where $i_p(\infty)$ is the current at short wavelengths where the absorption coefficient is very large. This equation will be discussed for two extreme values of the surface recombination velocity.

a) $s = 0$

The recombination rate at the surface is the same as whithin the volume. The equation shows that the current forms a level plateau at wavelengths shorter than the absorption edge, and no maximum in the spectral response is predicted. This is shown in figure 00.

b) $s >> \frac{L}{p}$

The carriers will recombine mainly near the surface. At short wavelengths, α is very large and decreases slowly with wavelength;thus a level, or slightly increasing plateau is predicted at short wavelengths. As the bandgap is approached, the absorption coefficient begins to decrease more rapidly; from the equation it may be seen that this has the effect of increasing the current equally as rapidly.

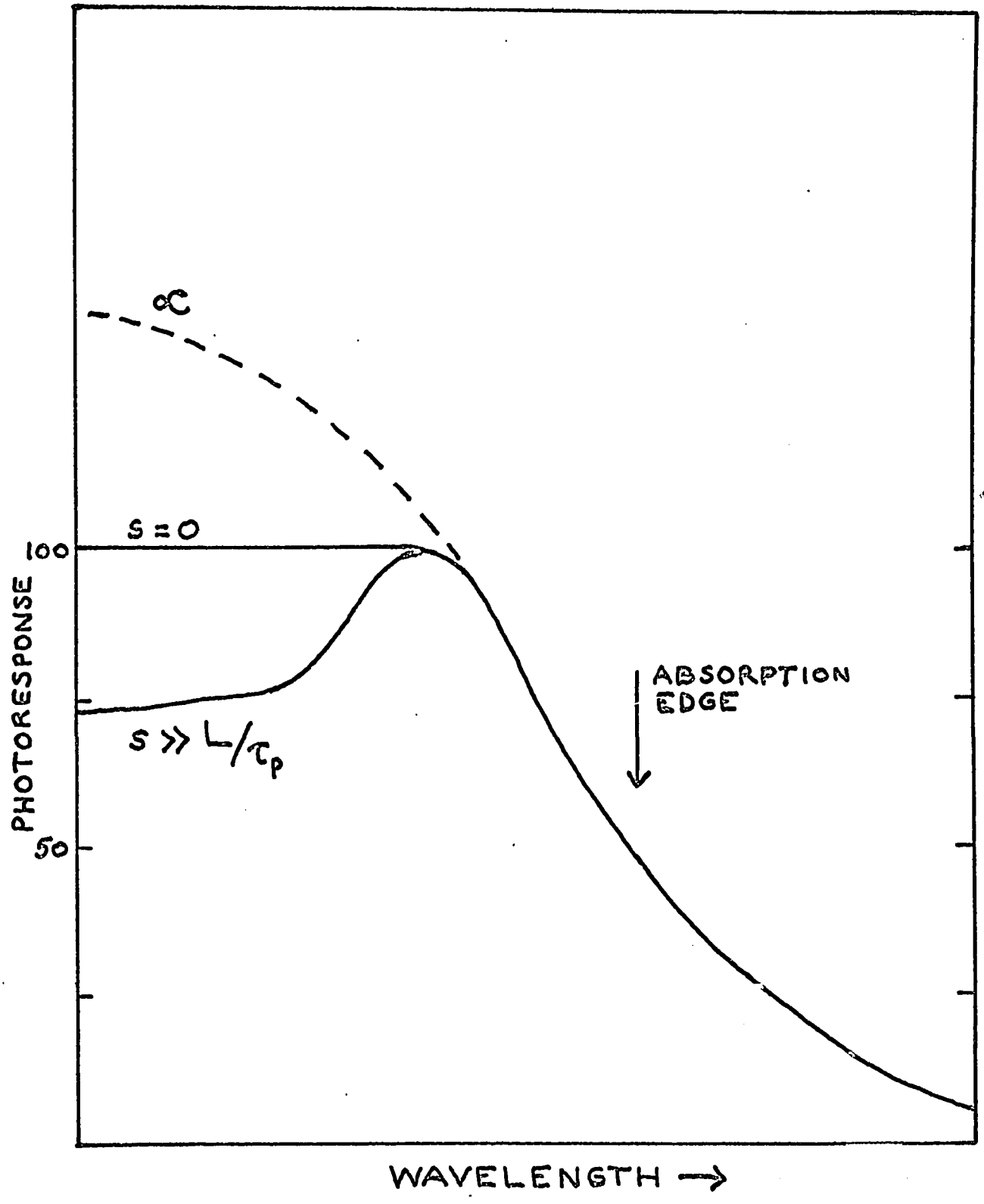

Fig. 00 VARIATION OF THE PHOTOCURRENT WITH WAVELENGTH for two extreme cases of the surface recombination velocity s. The variation of the absorption coefficient α is shown as well.

11.4 Photoresponse at wavelengths longer than the spectral peak

In the vicinity of the band edge and at longer wavelengths, Moss[4] has developed a model based on the observation that the response for many photoconductors has a maximum near the bandgap and decreases exponentially with wavelength beyond the maximum.

The spectral response in this region is postulated as

$$S(E) = \frac{1}{1 + \exp\{\beta(E_0 - E)\}} \qquad (2\text{-}16)$$

where E is the energy of the radiation, E_0 some "threshold" energy, and β a constant. This predicts a flat response at short wavelengths (similar to the case for s = 0 in the previous section) and an exponential fall with energy at longer wavelenghts. The photosensitivity curve for a typical semiconductor is shown in figure 0. The experimental results are more accurately represented by an exponential fall with wavelength (rather than energy) but the difference is seen to be small and becomes noticeable only at more than an order of magnitude down from the maximum of the response curve.

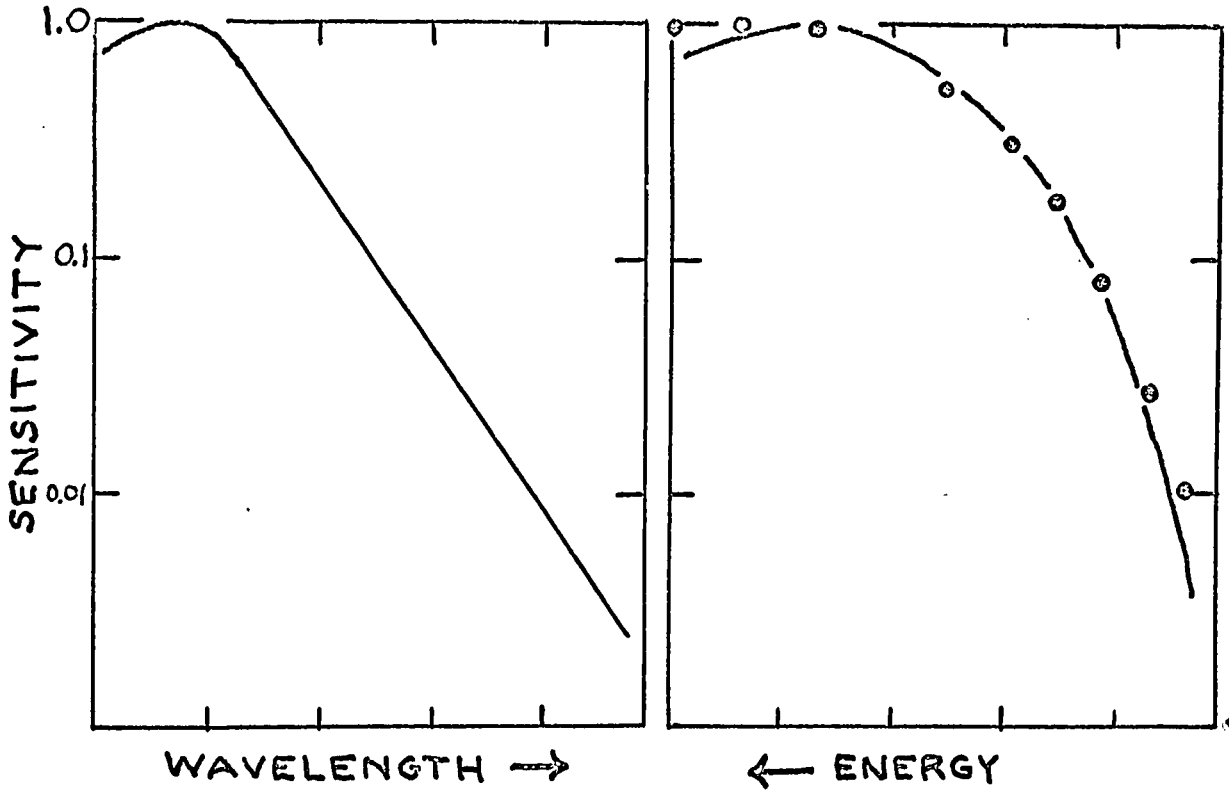

Spectral sensitivity curve for a typical semiconductor, plotted versus wavelength and quantum energy. Solid points are from the model (eq. (2-16))

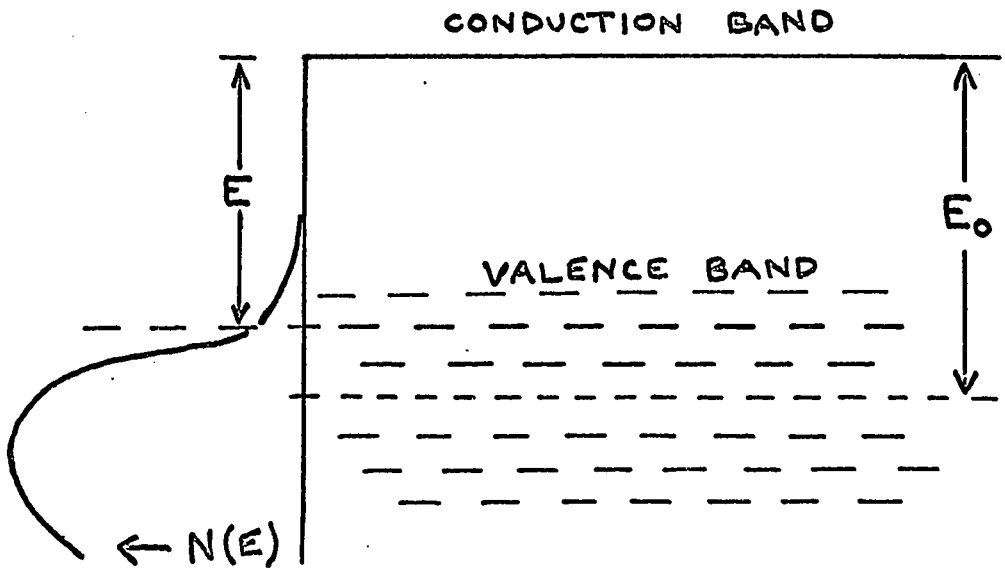

Fig. 0 MOSS' MODEL: Spectral curves and energy level scheme from T. S. Moss[4].

II.5 Moss' criterion for determining energy bandgap

Because of the exponential fall of sensitivity with wavelength, there is no significance in the longest wavelength at which photo-conductivity can be observed and there is no obvious threshold wavelenght. On the other hand, Moss[4] observes that thermal measurements (Hall Effect or conductivity) yield a definite value of activation energy. He then develops a criterion for determining the optical activation energy from its relation to this thermal activation energy. For the III-V compounds, there should be no difference in the thermal and optical activation energies on account of the homopolar nature of their bonding and the Franck-Condon principle.

In homopolar bonding, the valence electrons of nearest neighbour atoms form bonds, each consisting of two electrons with opposite spins. Bonding in a diamond lattice (as in germanium and silicon) is essentially homopolar; in the zinc blende lattice (the III-V semiconductors), the same arrangement of nearest neighbours is found, but the neighbours have unequal numbers of valence electrons due to the charge on the atomic cores differing from those of the diamond lattice by $\pm$ e. As a result, these compounds are primarily homopolar with a small heterpolar contribution[5].

The Franck-Condon principle may then be applied. It states that an optical excitation process takes place in a time interval

small compared with the period associated with lattice vibrations; atomic cores may be considered to remain at rest during this transition, relaxing later to a new equilibrium. Hence, the optical activation energy is larger than the thermal activation energy by this energy from the relaxation of the atomic cores[6]. In homopolar lattices, any atomic displacement occuring after an optical transition give off comparatively little energy and the optical and thermal activation energies are approximately equal.

Continuing with the model proposed by Moss[4], it is assumed that the varying sensitivity S(E) results from the distribution N(E) of energy levels in the valence band, from which the photoelectrons originate. With radiation of energy E_λ, the sensitivity will be proportional to the total number of states with energies lower than E_λ.

$$S(E) \sim \int_0^{E_\lambda} N(E)dE$$

$$N(E) = B \frac{dS(E)}{dE} \quad ; \qquad B = \text{constant} \tag{2-17}$$

and using eq. (2-16) for S(E),

$$N(E) = \frac{B\beta \exp\{\beta (E_0 - E)\}}{[1 + \exp\{\beta(E_0 - E)\}]^2} \tag{2-18}$$

From this expression for the distribution of levels, Moss calculates the number of electrons which will be present in the conduction band due to thermal excitation from the level E in the valence band (figure 0):

$$C\{N(E)\}^{1/2} \exp\left(-\frac{E}{2KT}\right) dE; \quad C = \text{constant} \qquad (2\text{-}19)$$

and the total number is

$$n = \int C\{N(E)\}^{1/2} \exp\left(-\frac{E}{2KT}\right) dE \qquad (2\text{-}20)$$

Substituting for N(E) from eq. (2-18) and solving gives

$$n = C\left(\frac{B}{\beta}\right)^{1/2} \frac{\pi}{\sin\pi a} \exp\left(\frac{-E_o}{2KT}\right) \qquad (2\text{-}21)$$

where

$$2a = 1 + \frac{1}{\beta KT}; \qquad 0 < a < 1 \qquad (2\text{-}22)$$

The condition on a is essentially a condition on the fitting parameter β, and is satisfied in this work. Eq. (2-21) corresponds to the expression in conductivity or the Hall effect for electrons excited into the conduction band with an activation energy W:

$$n = \frac{2(2\pi mKT)^{3/2}}{h^3} \exp\left(-\frac{W}{2KT}\right) \qquad (2\text{-}23)$$

Comparing eq. (2-21) and (2-23)

$$E_o = W \tag{2-24}$$

When E = W in eq. (2-16),

$$S(W) = \frac{1}{1 + \exp\{\beta (E_o - W)\}} = \frac{1}{2} \tag{2-25}$$

From this model, it is concluded that the optical activation energy is determined from the spectral photoresponse curve at that point where the sensitivity has fallen to half its maximum value. This criterion, and the method used to correct the response curves for and equal energy spectrum, will be demonstrated later for a particular sample.

CHAPTER III

EXPERIMENTAL

The equipment and the experimental procedure are discussed in this chapter. The light source, the monochromator and the optics are described first, followed by an outline of the electronic system. Finally, the cryostat is described and a typical experiment is outlined.

III.1 Light source

Several sources may be used in the infrared. The glowbar, Nernst filament, and gas mantle are compared with an ideal blackbody and with each other in a recent paper by Ramsey and Alishouse[7]. They conclude that these sources are quite comparable over the range from 1 to 14 microns. The Nernst filament was chosen for this experiment because of its size (about 25 mm x 2.5 mm) and convenience. Its spectral emission curve is quite broad and peaks around 1.2 microns.

The filament is mounted in a source housing (figure 1) which was designed by the author and made in the machine shop of the Physics Department. The strands of wire extending from each end of the filament are attached to small machine screws fixed near the tips of

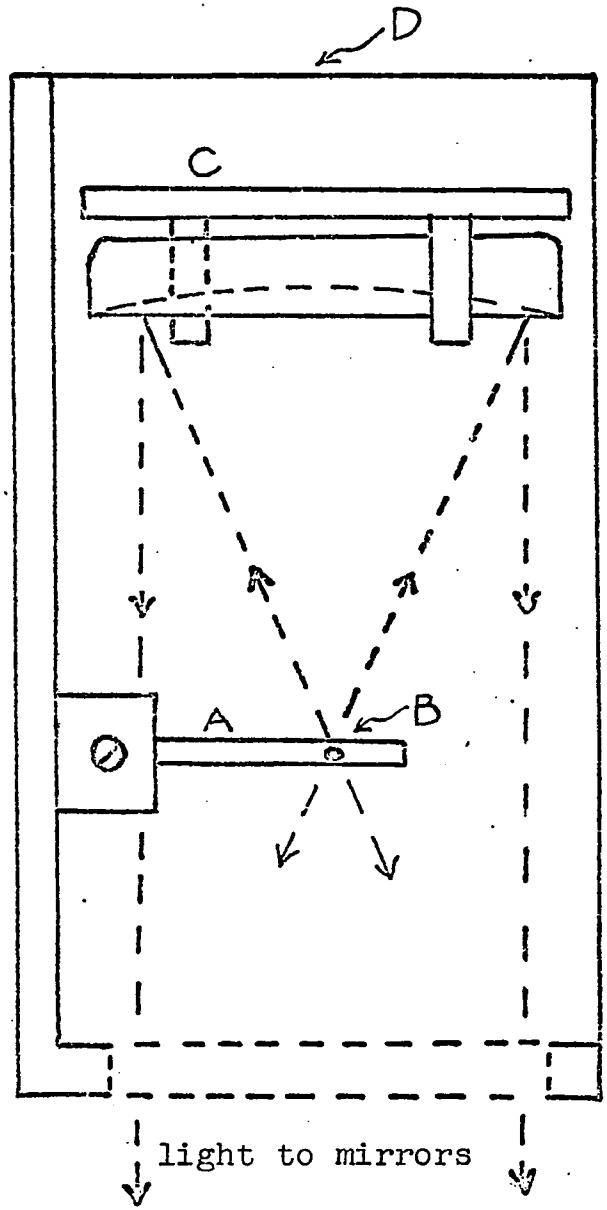

TOP VIEW

A. Adjustable brass rods
B. Nernst filament.
C. Mirror in adjustable holder
D. Enclosure forming Source house

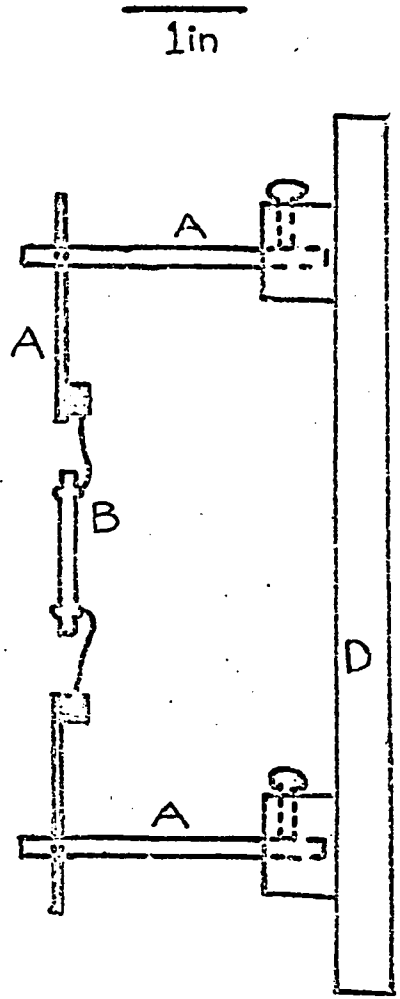

SIDE VIEW OF SUPPORT FOR NERNST FILAMENT

Fig. 1 SOURCE HOUSE

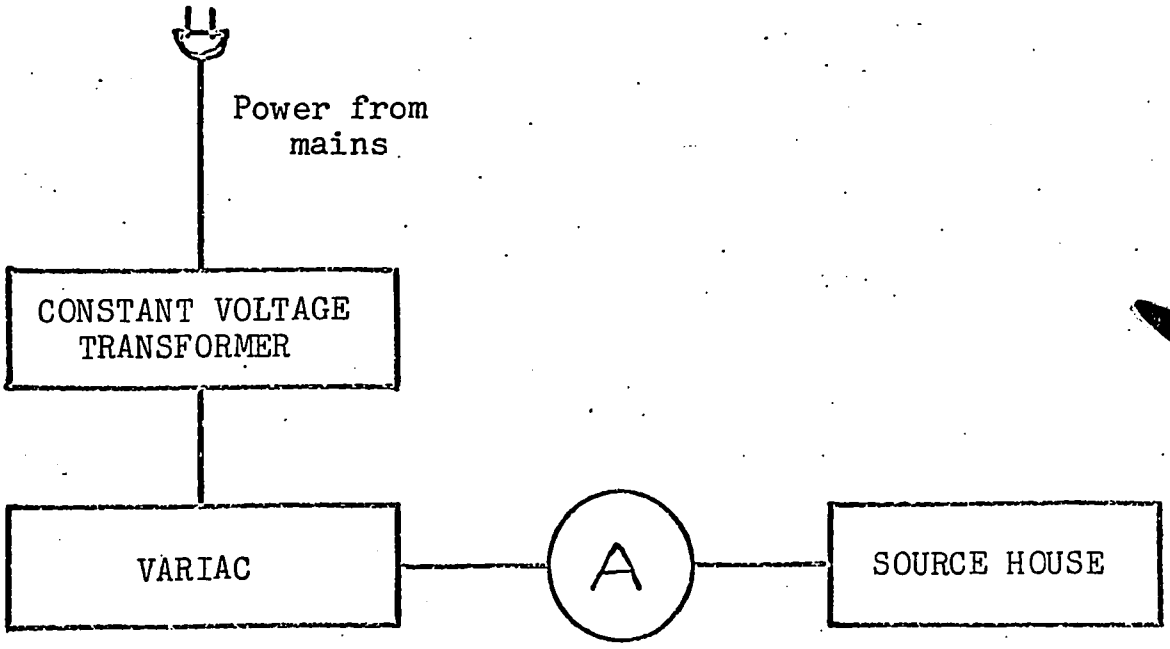

Fig. 2 POWER SUPPLY FOR NERNST FILAMENT

vertical brass rods. The filament can be adjusted vertically and transversely with these rods and set screws. Longitudinal movement is accomplished through mirror adjustment.

The rods conduct the power to the filament. A block diagram of the power supply is shown in figure 2. The filament has a high resistance when cold, and a negative temperature coefficient. Thus, a hand-held propane torch was used to preheat the filament on start-up and a stable power supply was needed to maintain it. A Sola constant voltage transformer, providing an output of 118 volts ± ½%, was followed by a variac and ammeter. The filament was found to be quite stable from 1 to 3 amps. In this work it was normally operated at 2.5 amps (about 225 watts) and a filament life in the hundreds of hours was obtained.

III.2 Monochromator

A SPEX model 1700 3/4 meter grating monochromator was used for this work. To achieve a spectral coverage from 0.8 to 7 microns, three Bausch and Lomb plane gratings of dimensions 102 mm square and 16 mm thick, were used; they were blazed at 1.6, 4, and 8 microns and had 600, 150, and 75 grooves/mm respectively. The intensity of the first order spectrum is greatest at the blaze wavelength and falls off to 50% of this value at two-third and twice the blaze wavelength.

Thus, the 1.6 micron grating is best used from about 1.0 to 3.2 microns wavelength. At a wavelength of 1.6 microns, this grating has a reciprocal linear dispersion of 20 Angstrom units/mm.

The entrance and exit slits can be varied in both height and width. The slit height is adjustable in steps from 50 mm to 2 mm by means of a 'fishtail'. It was set generally at 1 cm, a size which gave an image height at the output suitable for the sample dimensions. The slit width, continuously variable from 3 mm to 5 microns, determines the spectral bandpass of the monochromator. Using the 1.6 micron grating at a wavelength of 1.6 microns, a spectral bandpass of about 60 Angstrom units is obtained with a slit width of 3 mm. This represents a bandpass of about 1/3 of 1% of the centre wavelength (or equivalently, of the energy). The output power under these conditions was about 0.1 milliwatt. As no fine structure was expected in photoresponse curves studied in this work, the degradation of resolution with such a wide bandpass was of little importance. Operating with slits set at 3 mm provided better intensity, and this was of greater value in this work.

III.3 Optics

Figure 3 shows the layout of the optics. The source house and mirror mounts are bolted with adjustable fittings to a large ¼ inch

aluminum plate in front of the monochromator. This surface extends the versatility of the instrument in that simple adjustments can be made in the optics, especially at the output, to accommodate different experiments. Sufficient room is available for a cryostat and other equipment. A plane mirror is available, which, when mounted at the exit slit, would permit the exit beam to be 'swung' to different experiments.

The mirrors were made by the author under the direction of Mr. J. N. Cairns at the Optics Shops of the National Research Council. They were aluminized, and to maintain their high reflectivity and protect the surface from damage, a thin coat of silicon oxide was evaporated on top of the aluminum. The mirrors were mounted in adjustable aluminum holders.

The mirror inside the source house has a diameter D of 11 cm and a radius of curvature R of 26 cm. It is used to collect light over a solid angle of 45^{0} from the cylindrical filament, at its focus, and to reflect a parallel beam out of the source house. The following mirror (D = 11 cm, R = 150 cm.) focusses the image of the filament on the entrance slit of the monochromator. This mirror, with an f-number of 6.8, closely matches the f-number of the monochromator. This condition assures efficient use of the internal optics, especially the grating, and reduces scattered light. The beam diverging from the exit slit is focussed using another mirror (D = 9 cm, R = 40).

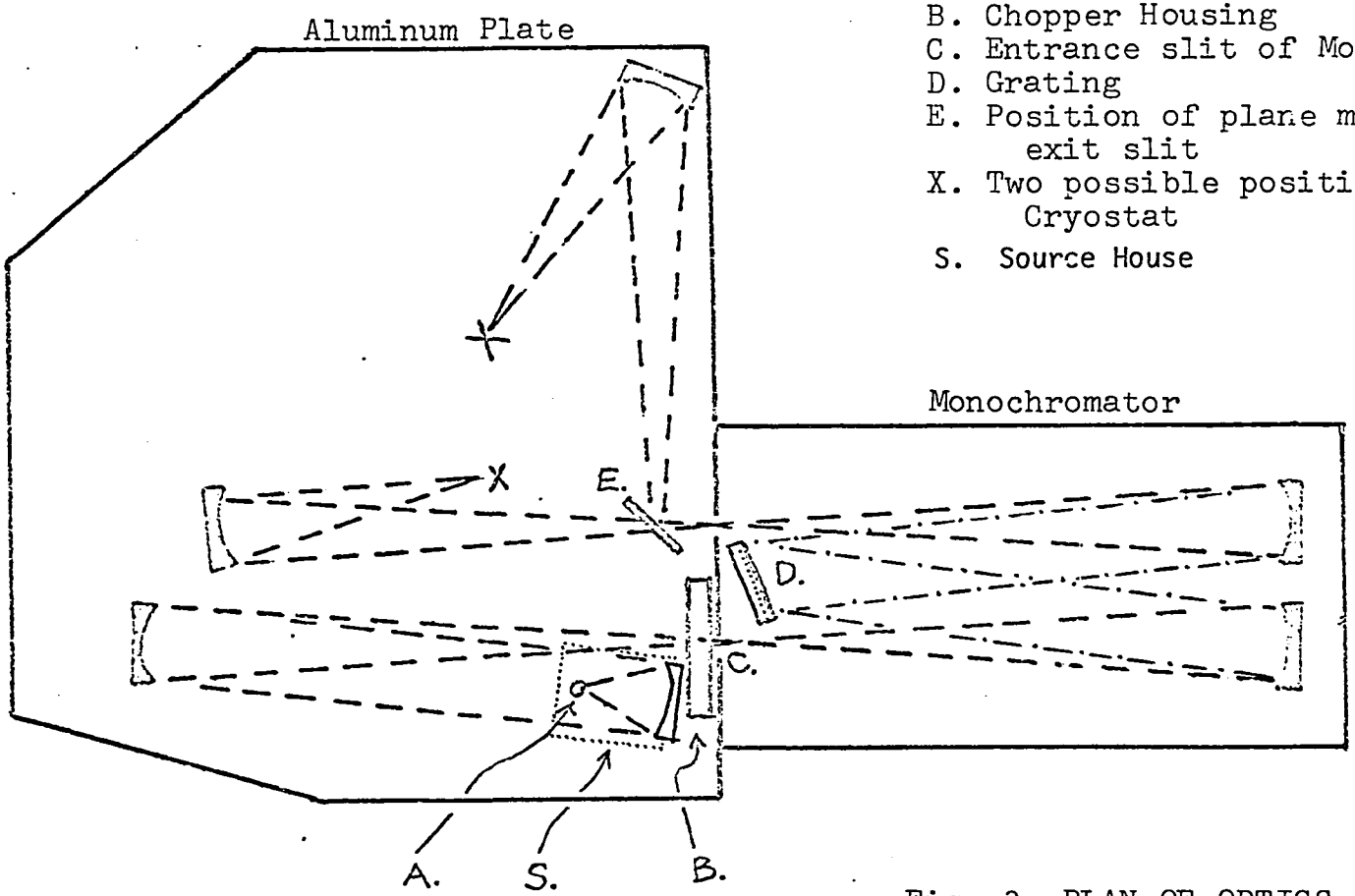

A. Nernst filament in Source House
B. Chopper Housing
C. Entrance slit of Monochromator
D. Grating
E. Position of plane mirror at exit slit
X. Two possible positions for the Cryostat
S. Source House

Fig. 3 PLAN OF OPTICS

1/10 scale

III.4 Filters and Spectral Intensity

The radiation at the exit of the monochromator consists of higher diffraction orders as well as the first order. Up to a few years ago there was no simple way of eliminating these orders, and hence prism monochromators were more popular in the infrared. However, filters have recently become available for these wavelengths.

Several of these new filters, designated here as #1, #2, and #4, were obtained from Optical Coating Laboratory, Inc. Two other filters of conventional manufacture (OX5 and CS2-64) were used as well. The transmission curves for several of these filters were obtained on a Beckman Spectrophotometer in the Chemistry department here. They are shown in the upper halves of figures 4, 5, and 6. The usefulness of these filters may be seen by referring to filter #2 in figure 5. This filter 'cuts on' quite sharply near 3.04 microns and transmits more than 60% up to 8 microns. Using this filter we obtain monochromatic radiation from about 3.1 to 6 microns; the second and higher orders of this range lie at 3 microns and lower, and are not transmitted.

The intensity of the monochromatic radiation available at the output depends on several factors: the spectral emission of the filament, the reflectance of the mirrors, the efficiency curve of the

grating, the transmission of the filter, and the absorption bands of the air. As we wish to correct experimental results for an equal energy spectrum, it is necessary to take these factors into account. Because of its flat response with energy, a thermal detector is most useful for obtaining intensity curves at the output. An Eppley air-type thermopile was used, and the resulting curves are shown below their corresponding filter curves in figures 4, 5, and 6, and in figures 7 and 8. The water absorption at 1.38 and 1.87 microns, carbon dioxide at 4.3 microns, and the water and carbon dioxide bands from 2.4 to 2.8 microns are visible on these curves. The method used to correct the photoresponse curves for equal intensity spectrum will be given later.

III.5 Chopper and Reference circuit

The very small signals expected from this and similar experiments can be detected only if the radiation is chopped, the electronics being tuned to pick up a signal at this frequency. The light chopper, shown in figure 9, was designed by the author and built in the machine shop.

The chopper was placed directly in front of the entrance slit, as shown in figure 3. It consists of a blade in which apertures are cut, and a suitable motor to drive it. Blades are available with one

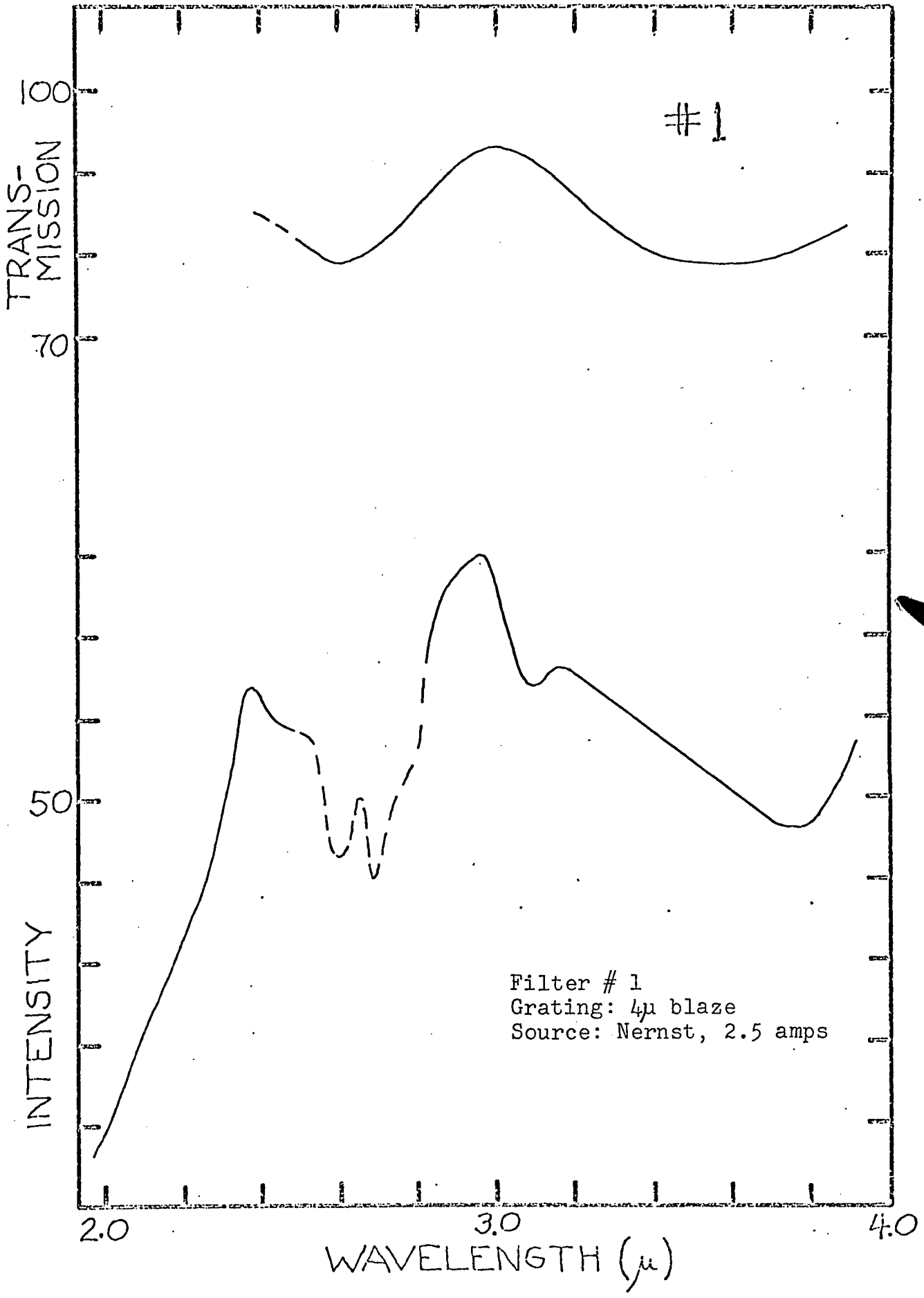

Fig. 4 UPPER: TRANSMISSION CURVE FOR FILTER # 1
LOWER: SPECTRAL INTENSITY OF SYSTEM

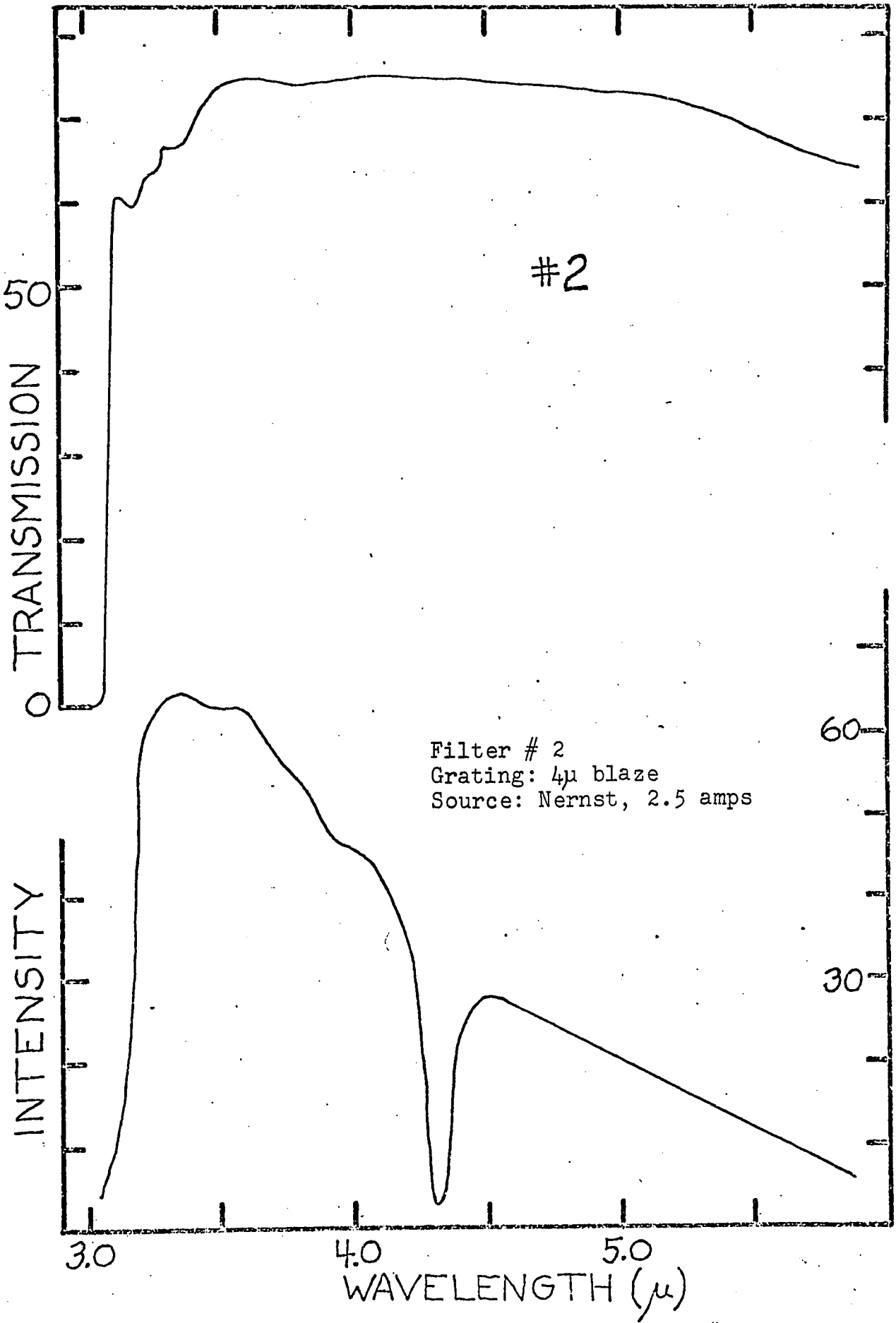

Fig. 5 UPPER: TRANSMISSION CURVE FOR FILTER # 2
LOWER: SPECTRAL INTENSITY OF SYSTEM

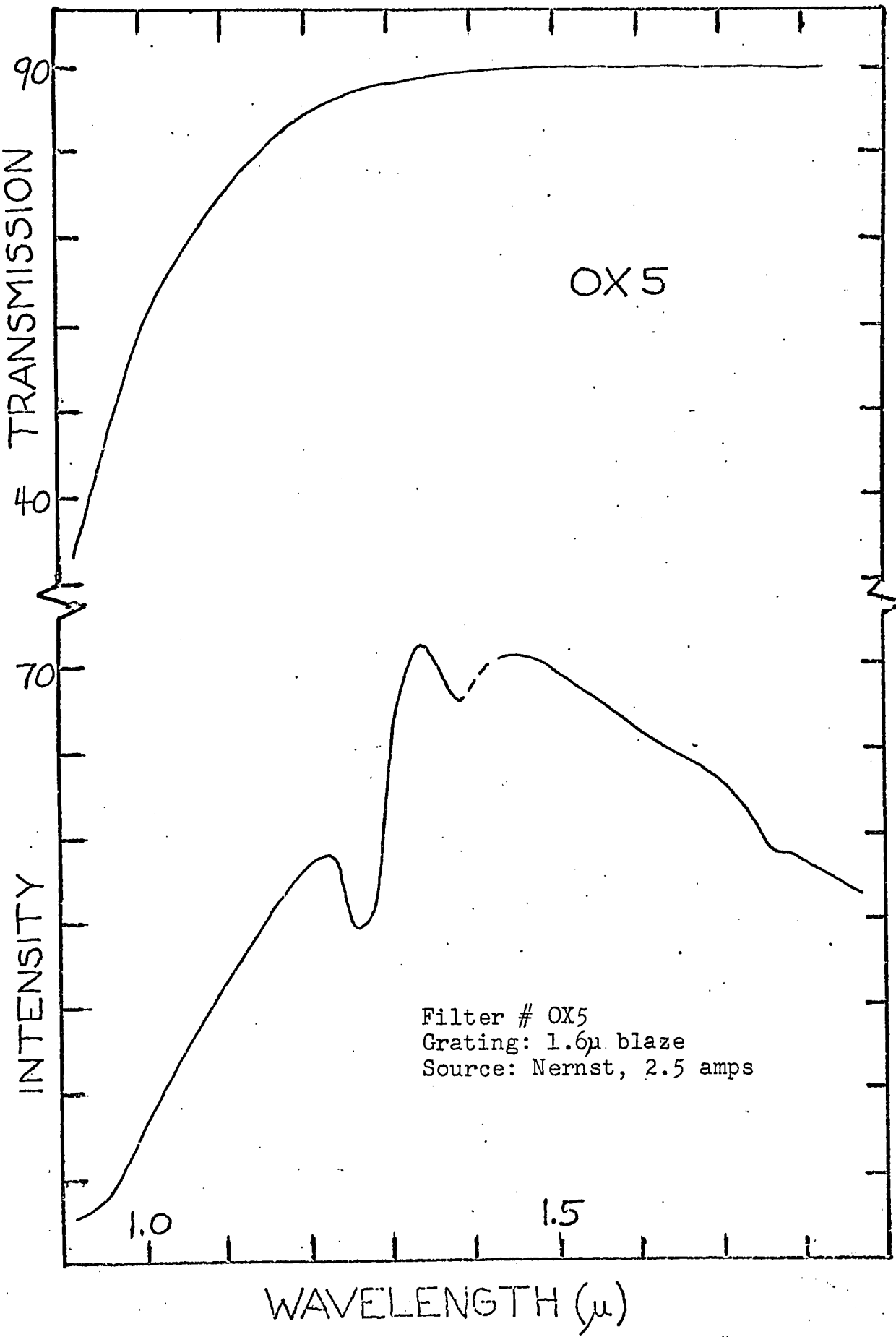

Fig. 6 UPPER: TRANSMISSION CURVE FOR FILTER # OX5
LOWER: SPECTRAL INTENSITY OF SYSTEM

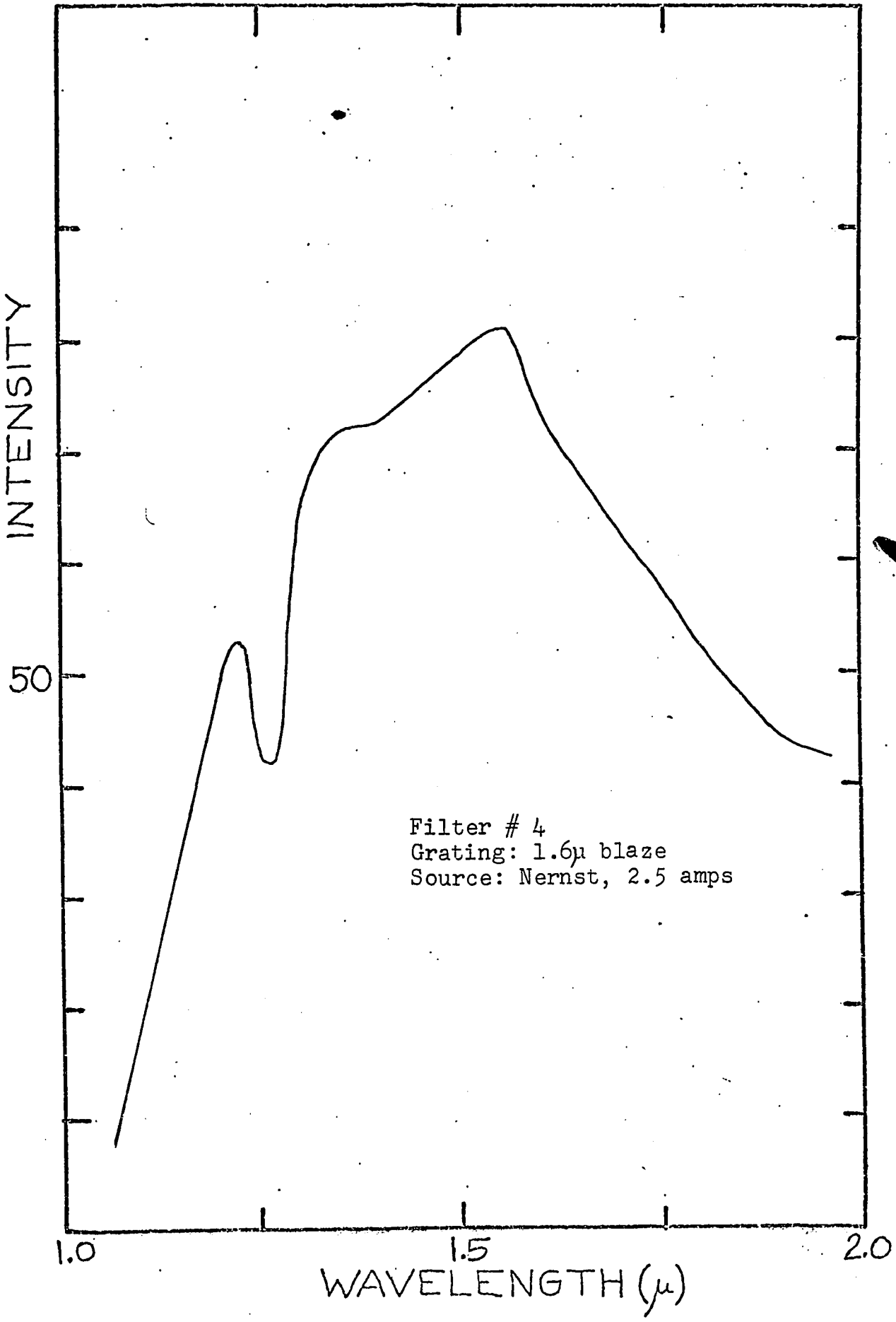

Fig. 7. SPECTRAL INTENSITY OF SYSTEM.

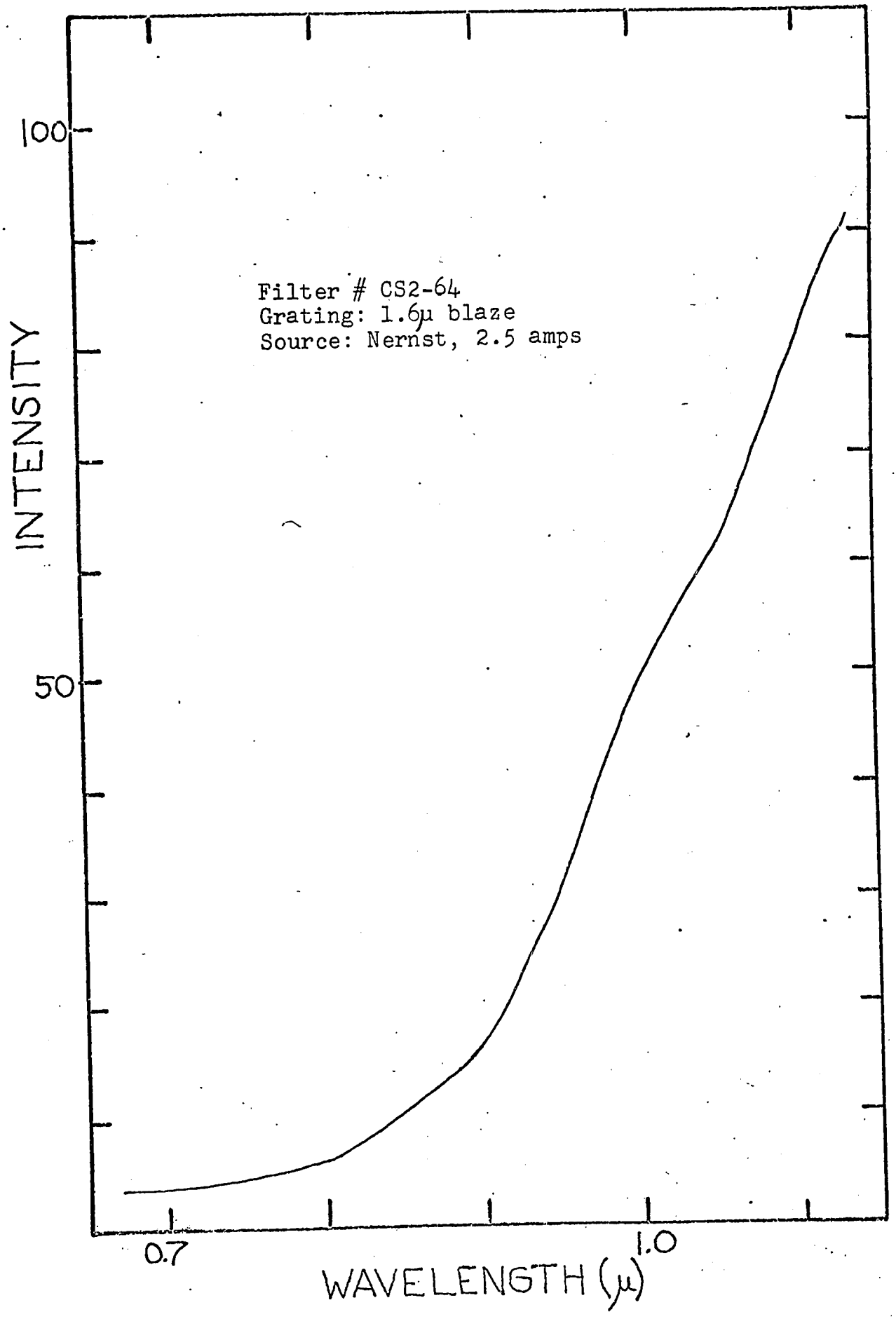

Fig. 8 SPECTRAL INTENSITY OF SYSTEM

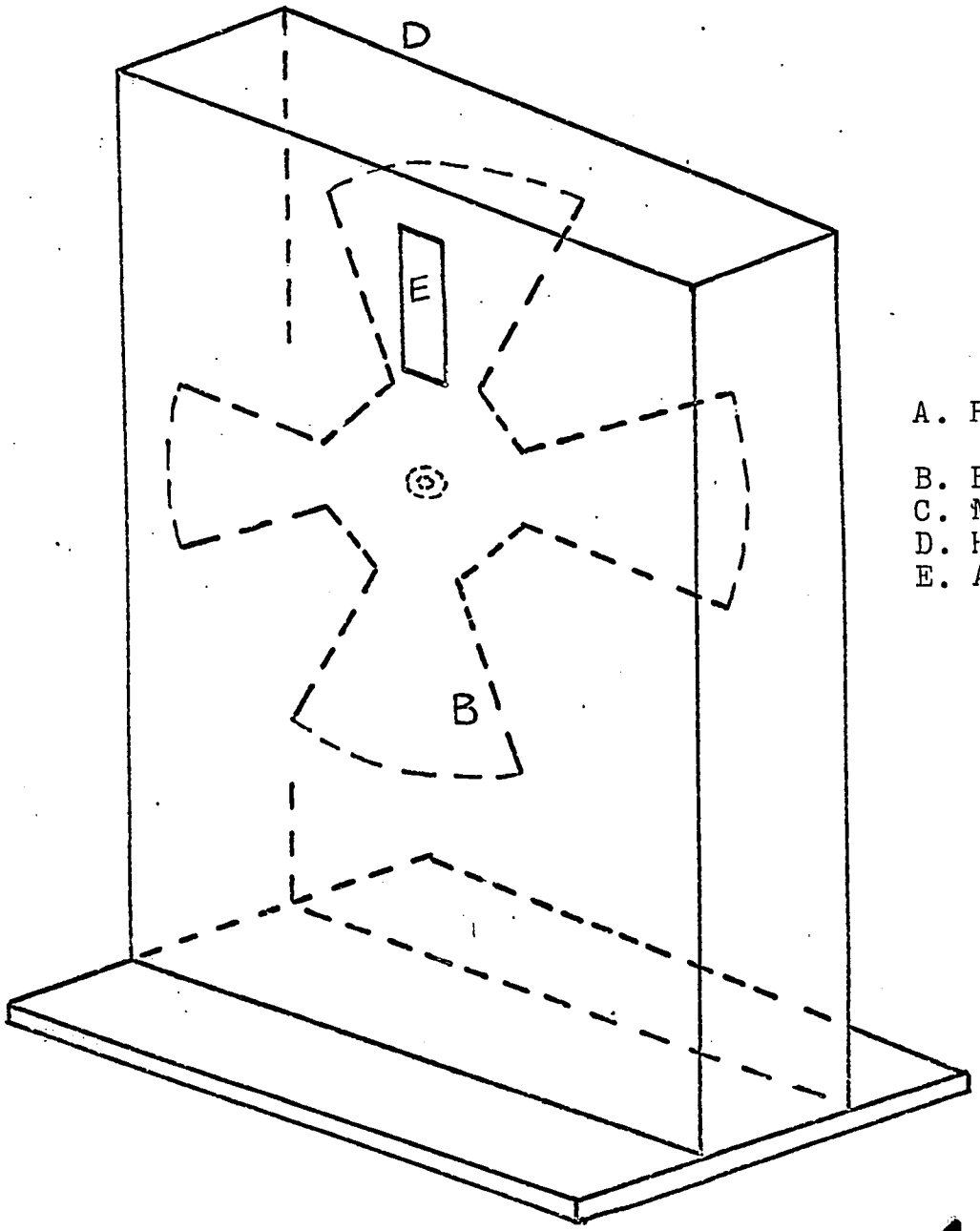

A. Reference cell
B. Blade
C. Motor
D. Housing
E. Aperture

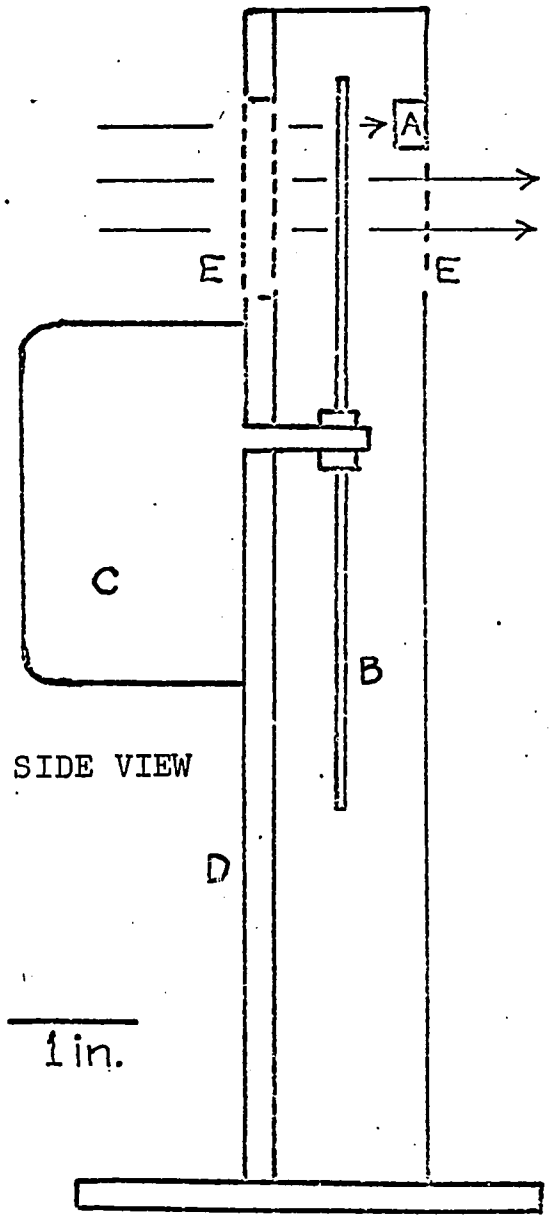

Fig. 9 LIGHT CHOPPER

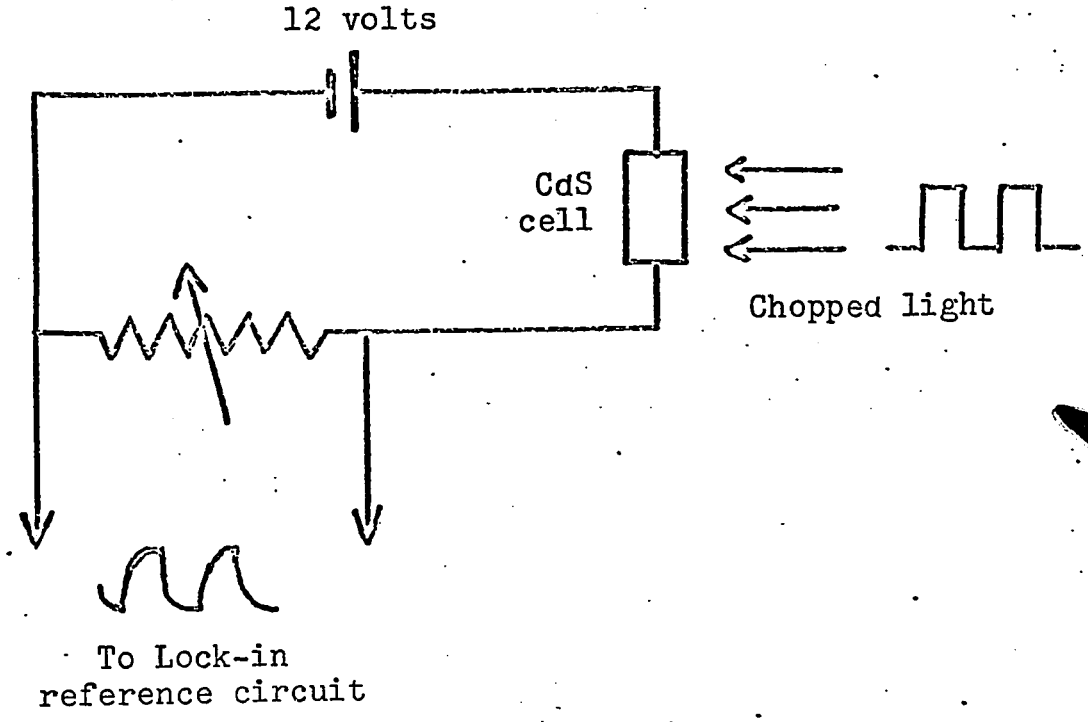

Fig. 10 REFERENCE CIRCUIT

aperture (a half circle), 8 and 17 apertures. With small Bodine synchronous motors of 100 rpm and 300 rpm, several discrete chopping frequencies were available, from 1.67 Hz to 85 Hz. Both motor and blade could be changed quickly. Generally a frequency of 13 1/3 Hz was used for the thermopile intensity runs, while 85 Hz was preferable for the photoconductive studies. The chopper housing would also accommodate a larger Leeds and Northrup motor, which could be driven over a continuous range of frequencies by a power oscillator. In this configuration, many experiments were done at 200 Hz. Frequencies were chosen to suit the experiment and the electronics; frequencies containing multiples of the 60 Hz power line were avoided.

A reference signal for the electronics was obtained by mounting a CdS photocell on the chopper housing where it receives a portion of the chopped radiation entering the monochromator. The circuit accompanying the cell is shown in figure 10. The variable resistance permits the output to be adjusted to provide at least 50 millivolts rms to the Lock-in amplifier.

III.6 Electronics

Many experiments involving the semiconductor alloys produce signals which are very small compared with the white noise present. In the photoconductivity measurements done in this work, this problem

arises from the relatively high carrier concentrations in 'as grown' material. The photocurrent is 6 or more orders of magnitude smaller than the dark current and an AC technique, plus high, stable gains must be used to recover such signals. A lock-in amplifier and a high gain low noise preamplifier form the heart of this detection system.

A block flow diagram for the electronics and associated equipment is shown in figure 11. Chopped monochromatic radiation falls on the sample in the cryostat. The photosignal and noise from the sample are picked up by the preamplifier from the sample control box. After initial wide band amplification of up to half a million times, the resulting signal and noise is put into a low Q selective amplifier tuned to the chopping frequency. This greatly attenuates the noise and prevents overloading of the Lock-in amplifier which follows. The Lock-in amplifier processes the reference signal from the chopper with the output of the selective amplifier and gives an output voltage proportional to the photosignal in the sample. A dual beam oscilloscope is useful in monitoring the system. The spectral distribution of the photoresponse is obtained by using the automatic wavelength scan of the monochromator and by recording the output of the Lock-in. The individual components will be described now in more detail.

The circuit diagram of the sample control box is shown in

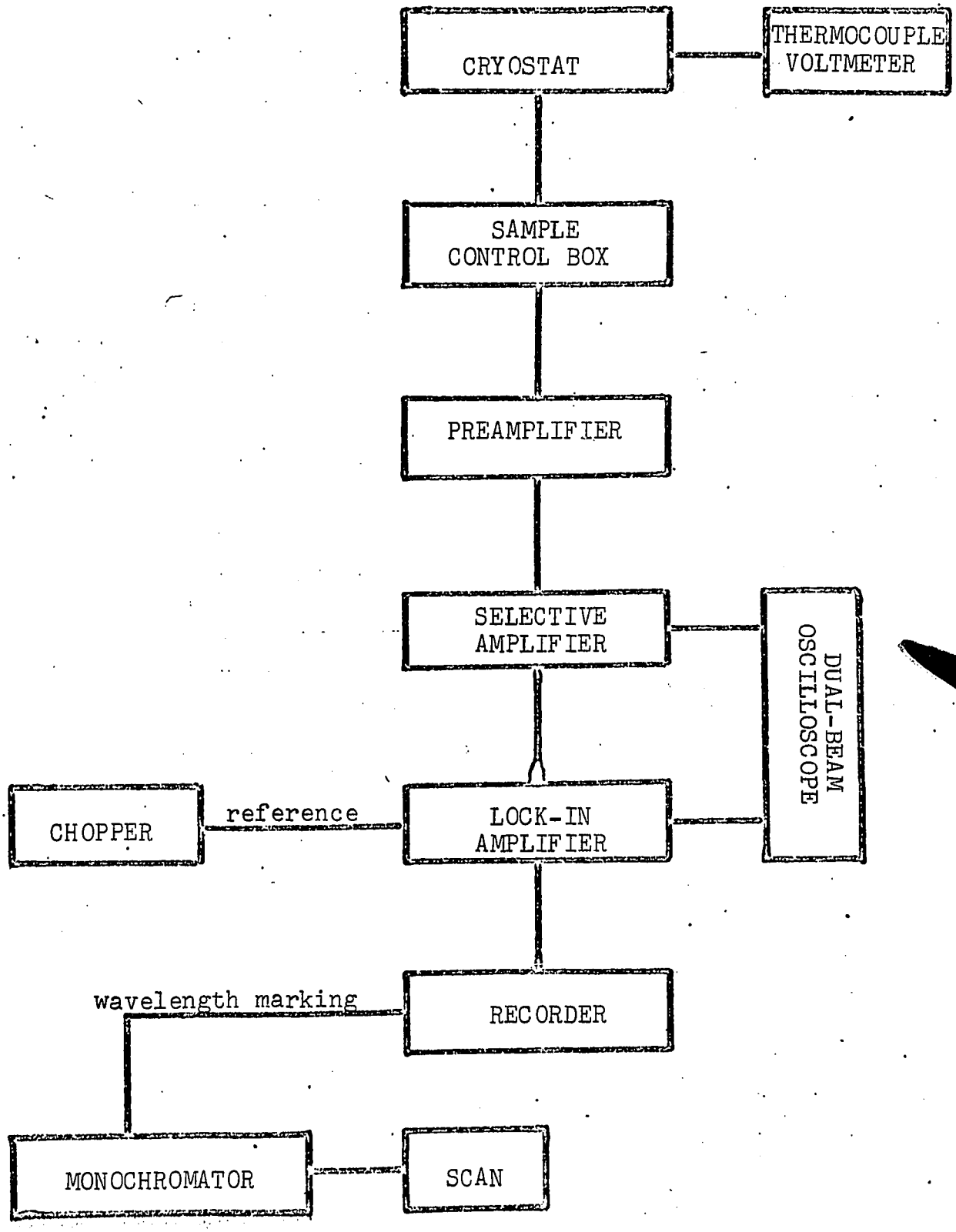

Fig. 11 BLOCK DIAGRAM OF THE EXPERIMENT

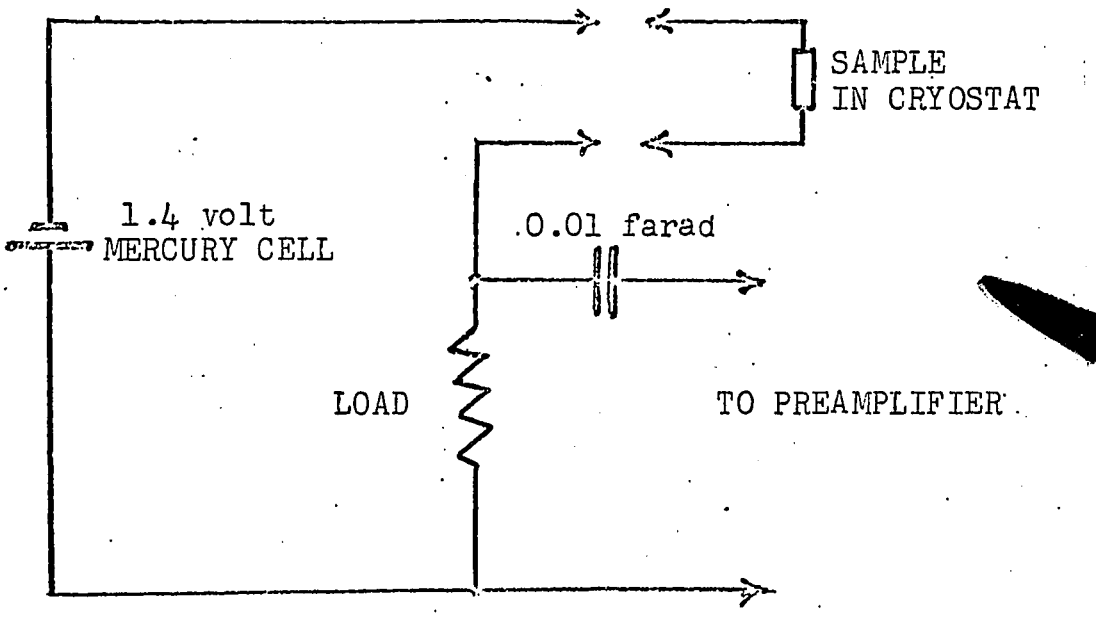

Fig. 12 SAMPLE CONTROL BOX

figure 12. The sample, mounted in the cryostat, is in series with a load of similar resistance, and a 1.4 volt mercury cell. The photosignal is taken across the load, and passed through a capacitor to the transformer input of the preamplifier. This 0.01 farad capacitor prevents the dark current from passing through the primary of the transformer and is large enough to pass the AC photosignal with little attenuation.

The preamplifier, a Princeton Applied Research model 213, has a direct and transformer-coupled input. The transformer input is used to match the low resistance of some samples to the higher input impedance of the amplifier. This is accomplished through the property of a transformer to give an effective impedance at the secondary equal to the impedance at the primary multiplied by the square of the turns ratio. For a given sample resistance, the chopping frequency and input mode required can be determined from the graph of noise contours provided with the preamplifier. In essentially all the photoconductivity experiments, a frequency of 85 or 200 Hz was employed, and the transformer input with a 1:354 turns ratio was used. This kept the operating points within the 1 dB noise contour.

A PAR model 210 Selective Amplifier followed the preamplifier. It was operated at the chopping frequency with a Q of 10 or 20, and this eliminated considerable noise. The Selective Amplifier was

operated with a gain of one. The Lock-in amplifier, a PAR model 220, is a phase-sensitive detector used in conjunction with a reference signal to give a very narrow bandwidth, and hence a high noise rejection. The frequency is tuned to the chopping frequency and the reference phase can be varied. The Lock-in gives a full scale output for an input of from 1 to 10 millivolts rms. Thus, with the overall amplification system and favourable experimental conditions, a signal of one nanovolt at the cryostat could, in theory, be detected. Signals in the tens of nanovolts were recorded satisfactorily.

The time constant of the Lock-in was set just sufficient to give an acceptable signal to noise ratio at the output. For any time constant, the wavelength scan rate of the monochromator was chosen so as not to produce undue relative lag of output signal to wavelength. The bandwidth of the entire electronics is determined by the time constant τ of the Lock-in.

$$\Delta f = \frac{1}{2\tau} \text{ Hz.}$$

Thus a time constant of 10 seconds gives a bandwidth of 0.05 Hz, while 1 second gives 0.5 Hz. The sharpness of this amplifier is emphasized when compared with the bandwidth of a conventional tuned circuit. With the Selective Amplifier, for instance, a Q of 100 gives a bandwidth of about 2 Hz at a 200 Hz centre frequency, or 20 Hz at a Q of 10.

Final output was taken on a Honeywell Electronik 193 strip chart recorder. Wavelength marks at desired intervals were put on the trace automatically by the output of a special circuit in the monochromator.

III.7 Cryostat

The portable cryostat used in this work was designed in this laboratory and made in the machine shop. A cut-away drawing is shown in figure 13. The material used for the well and outer tail piece is stainless steel. The inner tail is made of a solid piece of copper rod with a ¼ inch bore to within about ½ an inch of the bottom. A removeable copper sample holder screws into this tail, and is provided with electrical connections. The outer aluminum tail piece has two windows. A vacuum of 5×10^{-5} mm Hg can be reached easily; if the cryostat is then disconnected from the vacuum system and filled with liquid nitrogen, a temperature of $100^{o}K \pm 10^{o}K$ could be maintained at the tail for several hours. A second refrigerant of dry ice in equilibrium with acetone gave a temperature of $210 \pm 10^{o}K$.

A quartz window was used for experiments up to 4 microns; CaF_2 and KBr windows were used beyond this range.

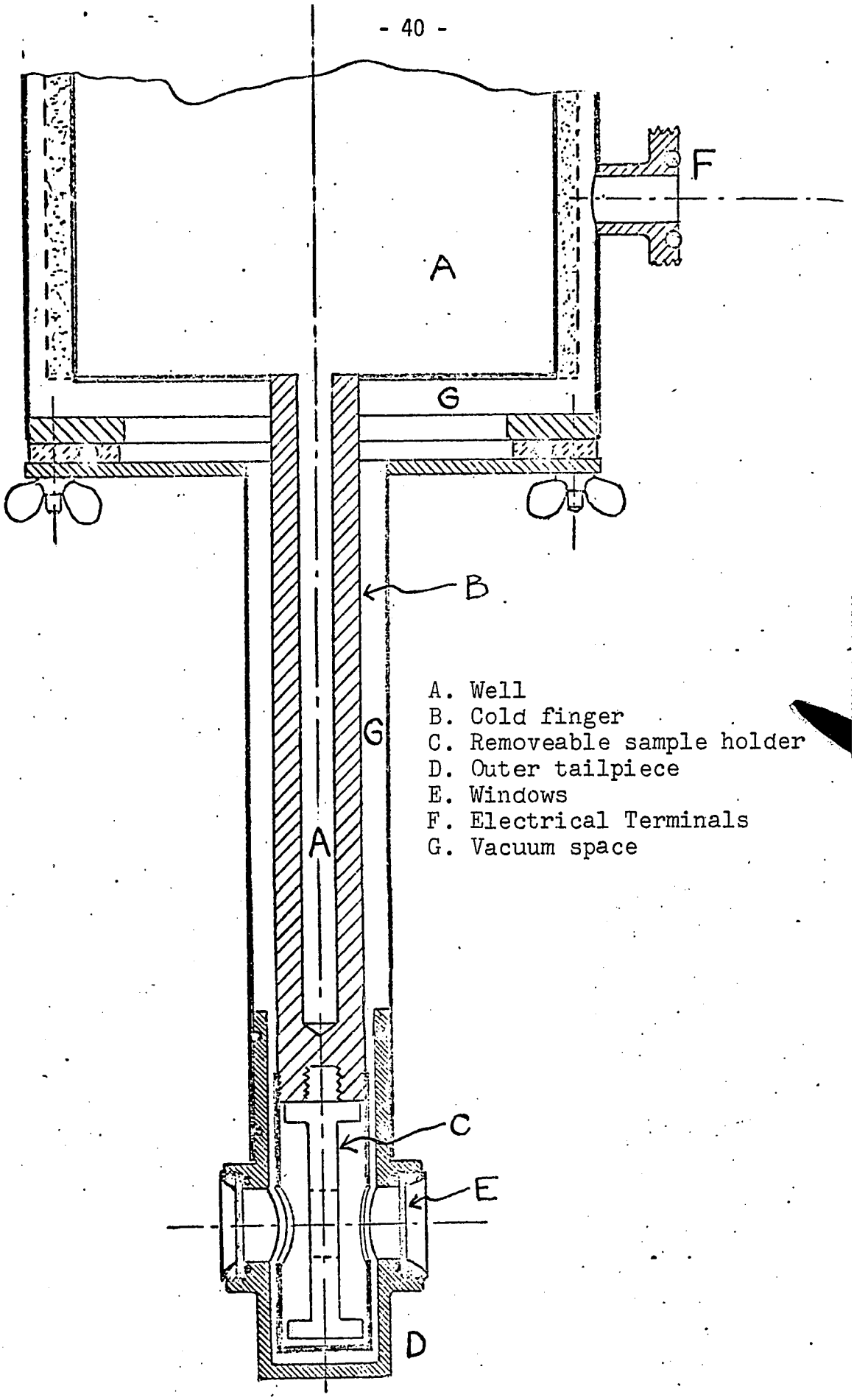

A. Well
B. Cold finger
C. Removeable sample holder
D. Outer tailpiece
E. Windows
F. Electrical Terminals
G. Vacuum space

Fig. 13 CUT-AWAY DRAWING OF CRYOSTAT

III.8 Experimental procedure

Some of the steps involved in an experimental run will be given in this section. Samples were first selected from an ingot, and polished. After applying contacts, the samples were mounted in the cryostat for the experiment, and the photoresponse curves were recorded. Finally the composition of each sample was determined by X-Rays.

i) Surface treatment

Slices were cut from the ingots using a carborundum saw. After mounting on a brass lapping block with wax, they were polished on a glass plate using 5 micron alumina powder and water, until a uniform surface appeared, or until the slice was of desired thickness. After removal from the tool, the slice was fixed with wax on a piece of 'arborite' for cutting to specimen size; spare pieces remaining were set aside for later X-ray powder photographs. Most of the samples at this stage were of the order of 7 mm x 2 mm and a bit less than a millimeter thick. An etch was used to chemically polish most of the samples in order to lessen surface damage. For InAs-rich specimens, a satisfactory etch was 1 H_2O : 3 H_2SO_4 : 1 H_2O_2; for GaAs-rich and GaSb-rich samples the etch used was 2 H_2O : 1 HNO_3 : 2 HCl.

ii) Contacts

To ensure that the response being measured was a property of the sample, and not a spurious contact effect, considerable care was exercised in applying the contacts and checking their ohmic behaviour. High purity indium was evaporated onto the ends of the top face, followed by alloying at 400^{o}C in a helium atmosphere for a few minutes. Small balls of 'Indalloy' solder, into which short pieces of gold wire had been melted, were then soldered onto the indium using a heat lamp. These contacts were found to be quite strong mechanically.

The ohmic character of the contacts, and the resistance of the sample were determined by the circuit shown in figure 14. Using the reversing switch, the resistance was determined for each direction of current through the sample, and for several different currents. Samples with good contacts closely followed Ohm's law.

iii) Mounting of the sample

After the contacts had been checked, the sample was mounted in the cryostat on the sapphire platelet using a thin film of selastic or vacuum grease as an adhesive. This assured electrical insulation and good thermal contact. The short pieces of gold wire were used to solder onto the electrical connectors at the tail of the cryostat.

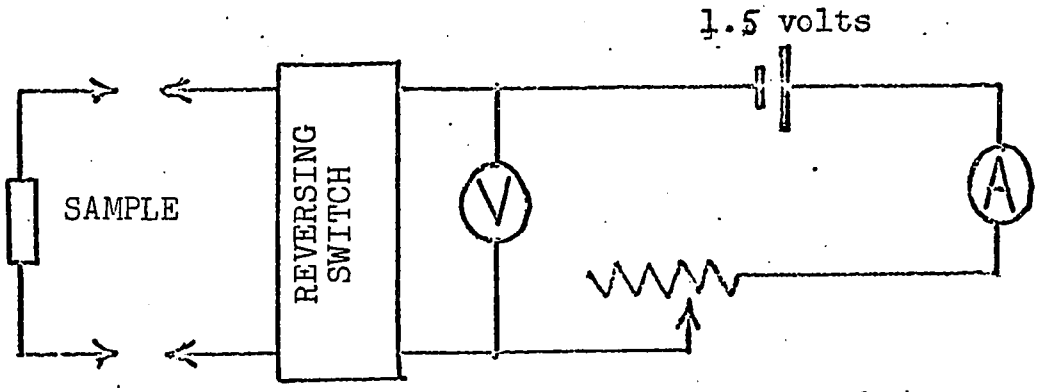

Fig. 14 CIRCUIT FOR CHECKING OHMIC BEHAVIOUR OF CONTACTS AND DETERMINING SAMPLE RESISTANCE

The various components and electronics were then connected as required with short lengths of shielded cable, and the three temperature runs were attempted. A copper-constantin thermocouple junction, positioned near the sample, was used to obtain the approximate temperature of the sample.

iv) Determining sample composition

The mole composition of each sample was known approximately from its position in the ingot. A more accurate value was obtained by taking X-Ray powder photographs of some of the material remaining from each slice, as mentioned earlier.

Analysis of the film was made a simple and rapid procedure through the use of graphs prepared by Mr. S. Rosenbaum. These graphs give the spacing of lines on the film for the zinc blende structure versus lattice constant. Because the graphs were made at the same scale as the film, direct reading of lattice spacing was obtained by placing the film over the graph.

Vegard's Law, which predicts a linear variation of lattice spacing with mole composition, was then applied. Previous work[8] has shown that GaAs-InAs follows this law closely; it was assumed valid for the limited region of interest in GaAs-GaSb. The compositions

determined by these techniques were considered accurate to within the unavoidable couple of percent error arising from the small composition range present in such a slice or sample.

CHAPTER IV

RESULTS AND DISCUSSION

The infrared system described in the previous chapter was used to study four alloy systems. The results for these will now be given. Only limited success was achieved with InAs-InSb. The photoresponse results for InAs were satisfactory and are presented in some detail. However, similar attempts on InAs-rich samples and on InSb were unsuccessful. The discussion of the problems encountered may be of help for future work. Next, photoresponse curves for the GaAs-InAs and GaAs-GaSb systems are given at three temperatures, and a qualitative discussion of the curves in terms of the theory developed earlier is presented. The energy bandgaps are plotted versus alloy composition. Finally, a brief outline of the attempt on GaSb-InSb is given.

IV.1 InAs-InSb

i) Ingot preparation

An ingot of this alloy was produced by the author. Amounts of InAs and InSb of usual laboratory purity were measured out to give an average mole composition of about 25% InAs. A quartz tube of ½ inch diameter was closed at one end in an oxygen-acetylene flame and the

material was put in. The flame was used to "neck" the tube such that the material was in a section about 5 inches long. The tube was then evacuated to about 10^{-4} mm. Hg and the neck sealed off.

The Horizontal Bridgman technique, described by Coderre[9], was used to make this alloy. The furnace consisted of two independent zones, one at 1000°C (higher than the melting point of InAs) and one at 475°C (just below the melting point of InSb). A steep temperature gradient between these zones was achieved with a narrow section of water-cooled baffles. The capsule containing the compounds was placed in a quartz carrier tube in the hot zone and was agitated several times to assist the mixing of the molten material. The carrier tube was motorized and was set to carry the capsule through the furnace at 0.6 cm. per day. The composition of the resulting ingot was obtained by powder X-ray photographs. The ingot was found to be polycrystalline and homogeneous in cross-section, with a composition gradient along its length. A graph of the composition profile of the ingot is given in figure 15. The very steep gradient in the middle of the ingot is a result of the wide liquidus-solidus separation for this alloy system.

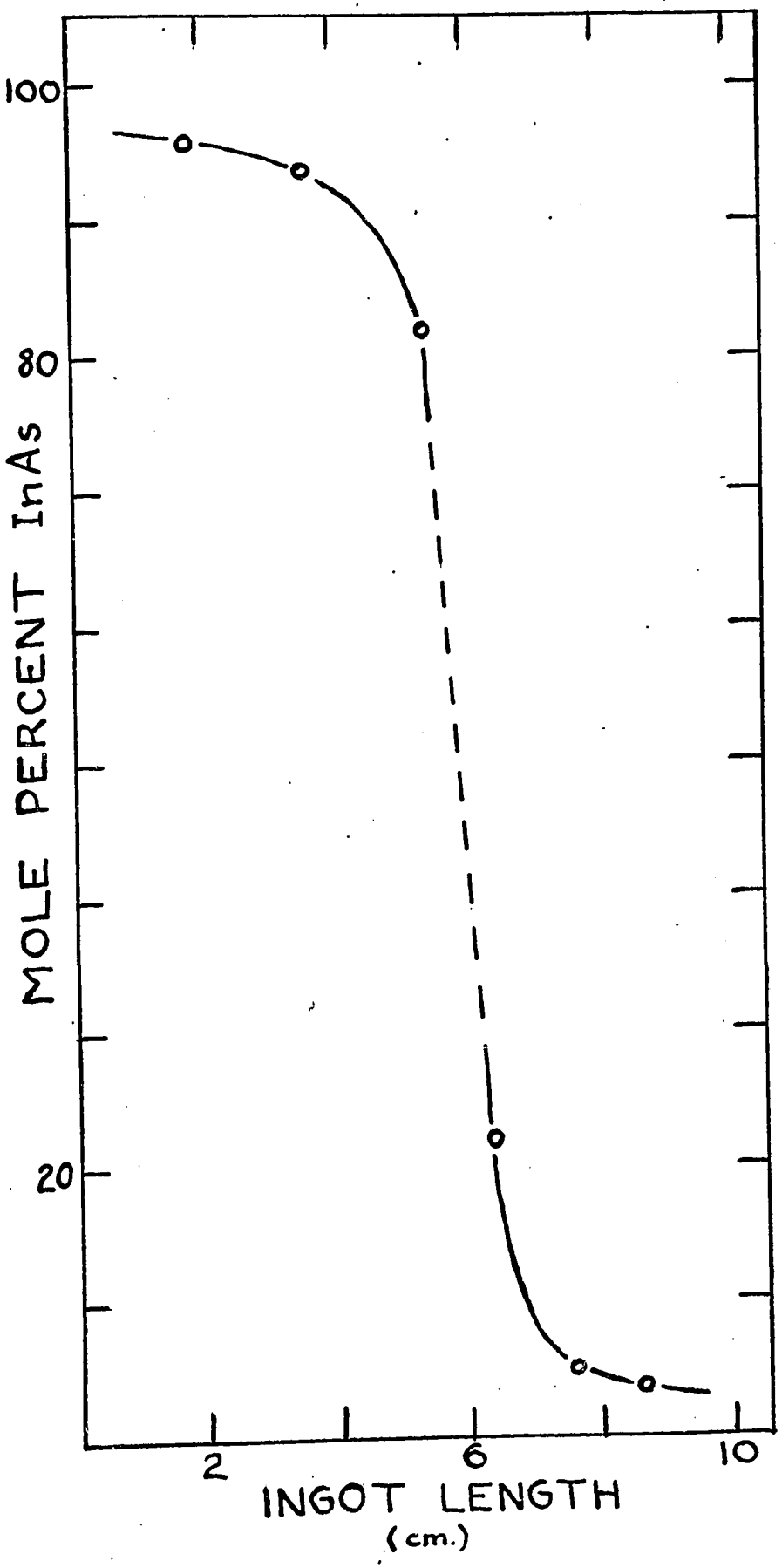

Fig. 15 COMPOSITION PROFILE OF InAs-InSb INGOT

ii) Sample preparation

Special techniques were required for these samples in addition to the methods outlined in Chapter III.8. To match the input impedance of the electronics, samples should have resistances of two ohms or more. The relatively low resistivity of InAs and InSb require the samples to be thin in order to achieve this.

Techniques suggested to the author by Mr. R. Senechal were used to make samples of the order of 100 microns thick. A slice about a millimeter thick of the desired material was cleaned in trichloroethylene and etched for several minutes in the InAs etch given in Chapter III.8; this was expected to remove saw damage. One surface was then ground with 5 micron alumina powder and carefully cleaned with cotton swabs and trichloroethylene before etching. This surface would constitute the back of the finished sample. The slice was mounted again on the lapping block with soft wax and the other surface was ground with 5 micron alumina until the sample had a thickness of 100 to 125 microns, as measured while on the lapping block using a special micrometer. The sample was removed from the block and carefully cleaned. Some samples were used without etching this front surface, while others were lightly etched. Finally, contacts were applied and checked by methods described previously. The thin samples that resulted were approximately 5 mm. x 2 mm. x 100 microns and had resistance of 2 to 5 ohms.

Although samples of such thickness are required for technical reasons, it is not apparent that the theory developed for "thick" samples (Chap. II.3) is still fully applicable. There the assumption was made that samples were sufficiently thicker than the diffusion length L so that generation-recombination processes were not influenced by the back surface.

The diffusion constant D is related through the Einstein relation to the mobility:

$$D_n = \frac{L_n^2}{\tau_n} = \frac{\mu_n KT}{e} \quad \text{or} \quad L_n = \left[\frac{\mu_n KT \tau_n}{e}\right]^{1/2} \tag{4-1}$$

Mobilities and lifetimes were not studied in this work, and it is difficult to make a close estimate of L_n. Of the materials studied, InAs and InSb have the largest mobilities, so they could be expected to give comparatively large values of L_n. Unfortunately, the techniques used for photoresponse measurements reauired InAs-rich samples to be thin (about 100 microns) in order that a photocurrent could be observed. The GaAs-rich samples, being almost a millimeter thick, and with generally much lower mobilities, probably can be considered thick, in the above context.

A rough estimate for L_n in InAs can be made. Mobility values vary somewhat but we take $\mu_n \sim 3\ m^2\ (V\text{-sec})^{-1}$. The volume lifetime for electrons (τ_n) is sensitive to impurities and imperfections, and processes such as trapping. Lacking sufficient experimental results from which τ_n can be measured, an estimated value of 10^{-7} seconds is taken. Calculation of L_n using these estimates yields a diffusion length of about 90 microns. Such an estimate is not conclusive, but results for InAs seem to follow the general shape predicted by the theory.

iii) Photoresponse results: InAs

Figure 16 shows the spectral response of an InAs sample at $100^{o}K$ and illustrates the method used to correct the curve for equal incident intensity. The thermopile graph, which gives the spectral intensity falling on the sample, is shown directly above. Moss' criterion (Chapter II.5) is used to determine the bandgap.

The photoresponse results at three temperatures for a particular sample are given in figure 17. With a bias of 1.4 volts, the peak signal before amplification at room temperature was 2×10^{-8} volts. Normally the response increased by an order of magnitude at lower temperatures; however, in this graph the vertical axis is arbitrary. The axes have been expanded as much as possible in order to illustrate the qualitative correspondence between the general shape of each curve and the theory given in Chapter II. The curve at wavelenghts shorter than the spectral peak is determined largely by the surface recombination velocity s, or equivalently, by the lifetime τ of the carriers in the surface layer. In this region, the lower response relative to the peak is evidence for a moderately large value of s and for a carrier surface lifetime smaller than the volume lifetime. The gently increasing response as the peak is approached was predicted as well in Chapter II.3, and arises from the decrease of the absorption constant as the band edge is approached. Experimentally, surface treatment governs response in this region.

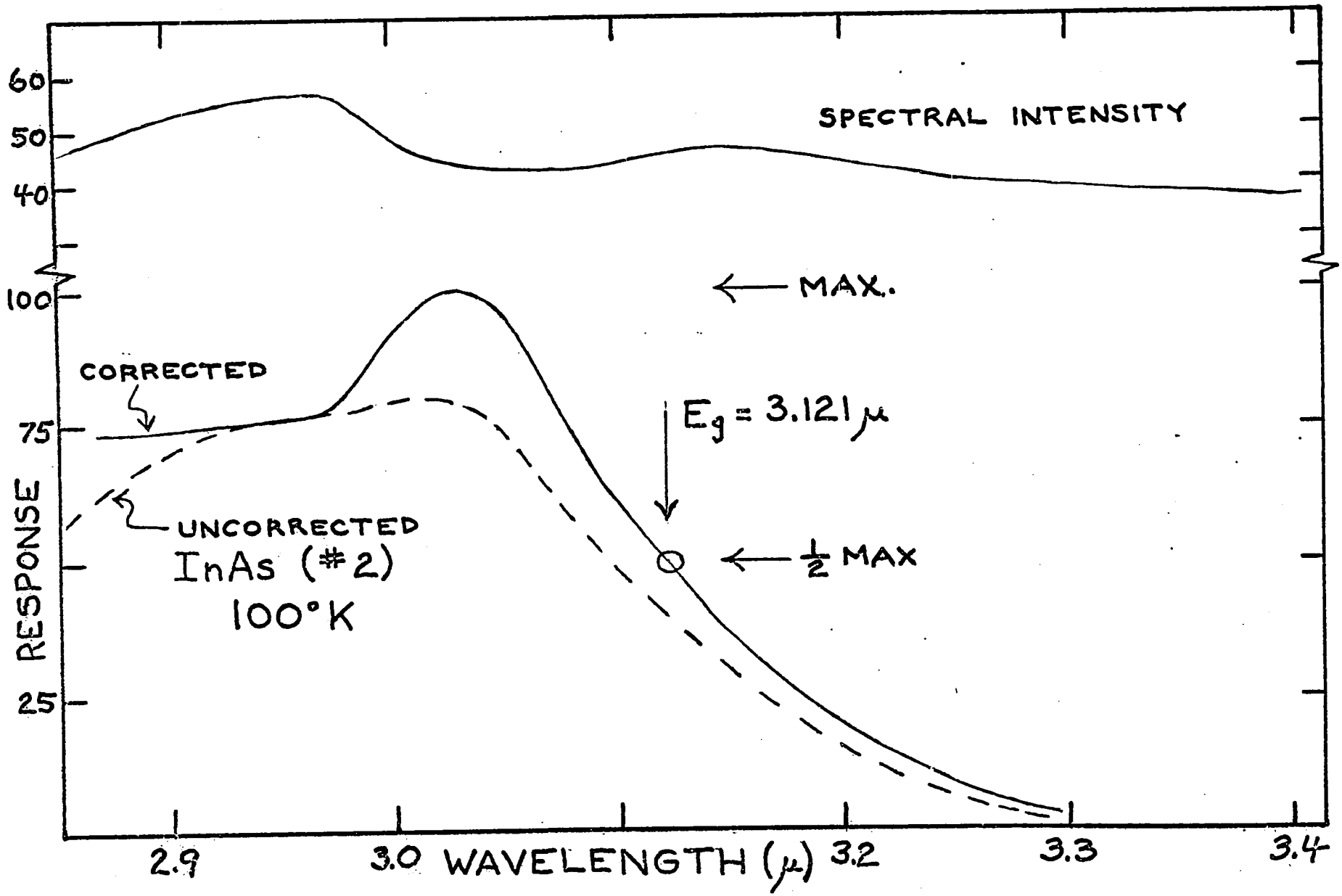

Fig. 16 METHOD OF CORRECTING PHOTORESPONSE CURVES FOR EQUAL INCIDENT INTENSITY AND DETERMINING THE OPTICAL BANDGAP

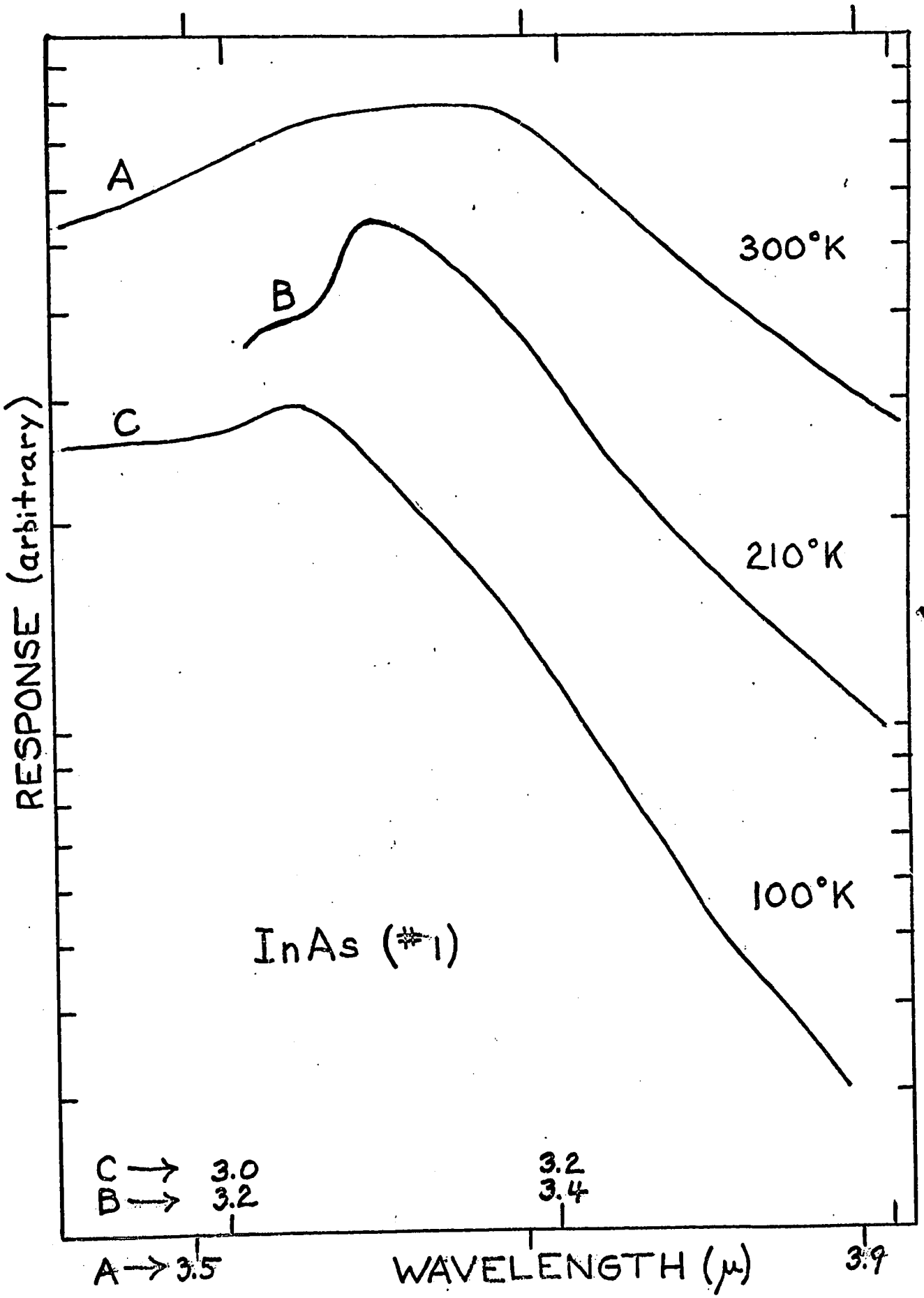

Fig. 17 PHOTORESPONSE CURVES FOR InAs

The ordinates of the curves bear no relationship to each other.

At wavelengths longer than the spectral peak, the response falls off exponentially for more than an order of magnitude. Deviations occur at lower values because of the increased difficulty in measuring these smaller signals. Such exponential decay was the basis of Moss' theory (Chapter II.4).

Photoresponse studies were made on three different samples of InAs. Optical bandgap values E_g determined for these are presented in Table II, together with recent generally accepted values of the bandgap[10].

iv) Photoresponse studies: InSb

Almost no success was met with InSb, but an outline of the techniques tried may be useful for other workers. No photoresponse was obtained for InSb samples prepared by the methods used for InAs, so a substantially different approach to sample preparation was taken. If commercially available polycrystalline material is fractured, the crystallites will split along directions of cleavage; from the broken material it is possible to choose a piece with a cleaved surface of 5 millimeters or more in one dimension. It was thought that this surface would possess less damage than a mechanically polished one.

TABLE II

OPTICAL BANDGAP VALUES FOR THE COMPOUNDS

Energy values are given in electron volts. Bandgaps for the three samples of InAs are shown separately, and averaged. Values in parenthesis are the most recent generally accepted values (Long[10])

SAMPLE	77°K	100°K	210°K	300°K
InAs #1		0.391 0.390 0.401	0.366	0.328
InAs #2		0.397		
InAs #3		0.385 (a) 0.387		0.334
Average InAs	(0.41)	0.395	0.366	0.331 (0.35)
GaAs	(1.49-1.53) (b)	1.46	1.42	1.41 (1.37-1.42) (b)
GaSb	(0.77-0.82) (b)	0.788	0.712	0.676 (0.70-0.74) (b)

Note: (a) Not included in average; sample confirmed to be in poor thermal contact with cryostat

(b) Accepted values uncertain; most optical data agree with first value, while more recent references give the second

A sample of suitable dimensions was cut from this irregular piece with the 'cleaved' surface as a face, and the other side was ground with alumina powder to obtain a thickness of about 125 microns. When contacts were applied, the resistance was one ohm. A response was obtained around 5 to 6 microns wavelength at liquid nitrogen temperature, but the noise level was high and could not be reduced to an acceptable level. The difficulties could be attributed to a couple of factors. First, the intensity available from this monochromatic system at 6 microns is down by more than a factor of 5 from that at 3 microns. Second sample resistance should be at least 2 ohms to provide a favourable match for the electronics.

v) Photoresponse results: samples from the alloy range

Using the same techniques of preparation as for InAs, measurements were attempted without success on several samples from the InAs-rich end of the ingot described above. The noise level was very high in all cases and masked any signal which may have been present. Since the method of preparation and the contacts were successful for InAs, it is concluded that the material itself is likely responsible for this noise. The alloy material did not appear as mechanically sound as the InAs, and considerably more difficulty was experienced in preparing thin samples. This may be due to the polycrystalline nature of this ingot.

Whereas the typical size of the crystallites in the InAs and InSb material is of the order of several millimeters, in the alloy they were much smaller, perhaps a millimeter.

IV.2 GaAs-InAs

i) Ingots

The samples were taken from ingots made previously in this laboratory by Thomas[11] and Coderre[12]. Prior electrical measurements indicated they were n-type with carrier concentrations from 5.0×10^{16} cm^{-3} to 2.5×10^{18} cm^{-3}. The sample preparation methods outlined in Chapter III.8 were found to be satisfactory for this system.

ii) Photoresponse results

The curves in the upper part of figure 18 give the spectral response at three temperatures for a sample of 75 mole percent GaAs (written conveniently as $Ga_{.75}In_{.25}As$). With a bias of 1.4 volts, the peak signal at room temperature before amplification was 7×10^{-6} volts. This maximum response increases about an order of magnitude at lower temperatures, but these and similar curves are normalized to 100. Since the temperature coefficient of bandgap is negative for these compounds, the spectral response curves for the alloy shift to shorter wavelengths with decreasing temperature.

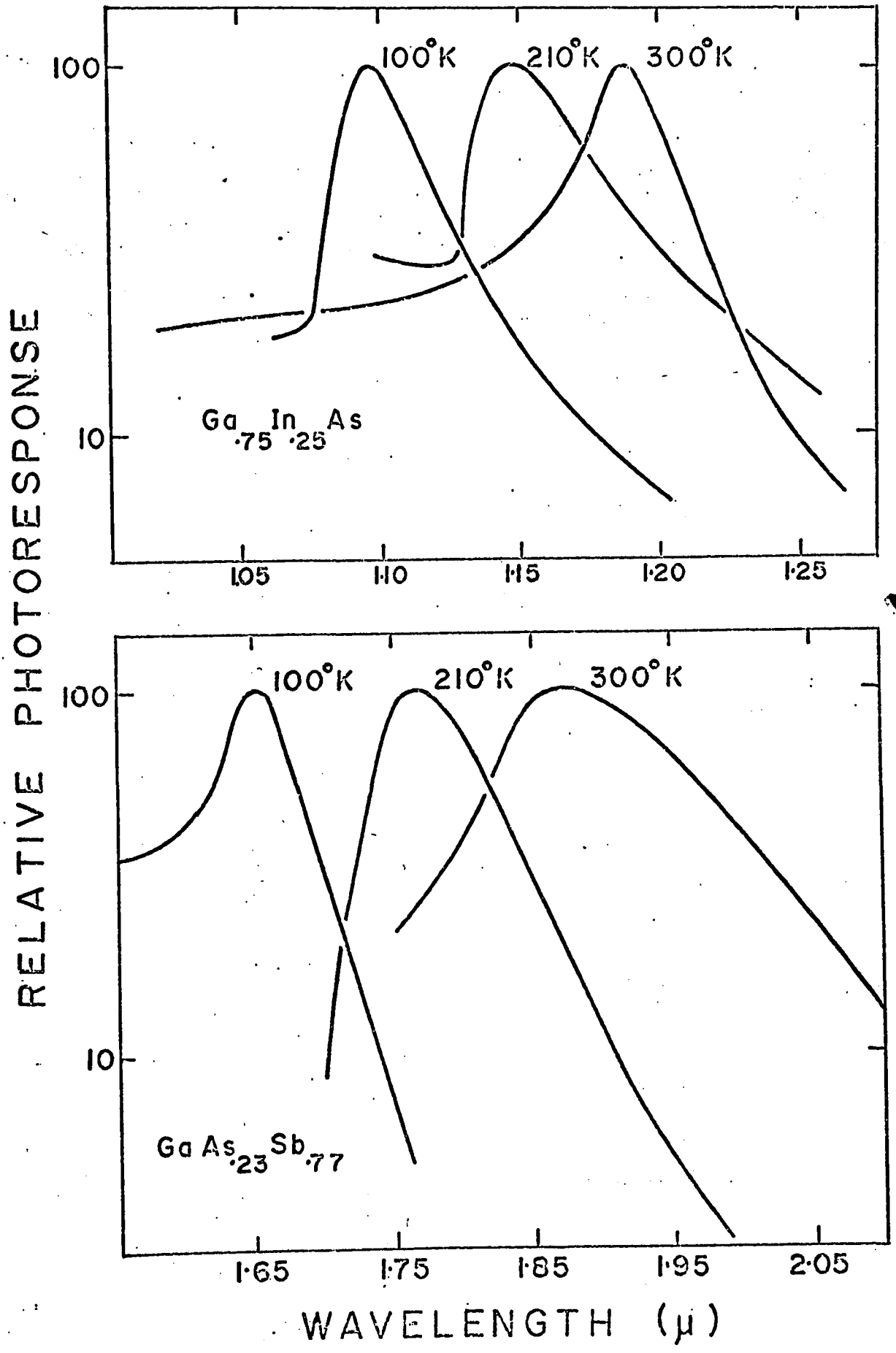

Fig. 18 PHOTORESPONSE CURVES

Curves for the remaining samples at the same temperatures are given in figures 19, 20 and 21 at a smaller scale. These curves exhibit the qualitative behaviour predicted by theory, as discussed previously for InAs. However, there are additional points worth mentioning. First, the considerable variation in the short wavelength responses from one sample to another is evidence for varying surface recombination velocities. Experimentally, this arises from the surface preparation differing somewhat among the samples. For semi-insulating GaAs, Milner-Brown[13] tried different surface treatments on the same sample and found the short wavelength photocurrent to depend on the surface. Second, all samples show the characteristic sharp exponential decay with wavelength. Finally, the spread of photoresponse curves across the alloy range is a first indication of their potential as variable threshold detectors. Further discussion of these curves in light of their possible use in infrared detection will be given in Chapter V.

iii) Bandgap values

The smooth variation of the optical energy gap E_g with mole fraction is shown explicitly in figure 22 at room temperature, and in figures 23 and 24 at $210^{o}K$ and $100^{o}K$ respectively. Results of other workers are shown as well. Those of Wrobel and Levinstein[2] were obtained from transmission measurements, while those of Thomas[14] were calculated from absorption curves. Coderre's[15] values were derived from Hall

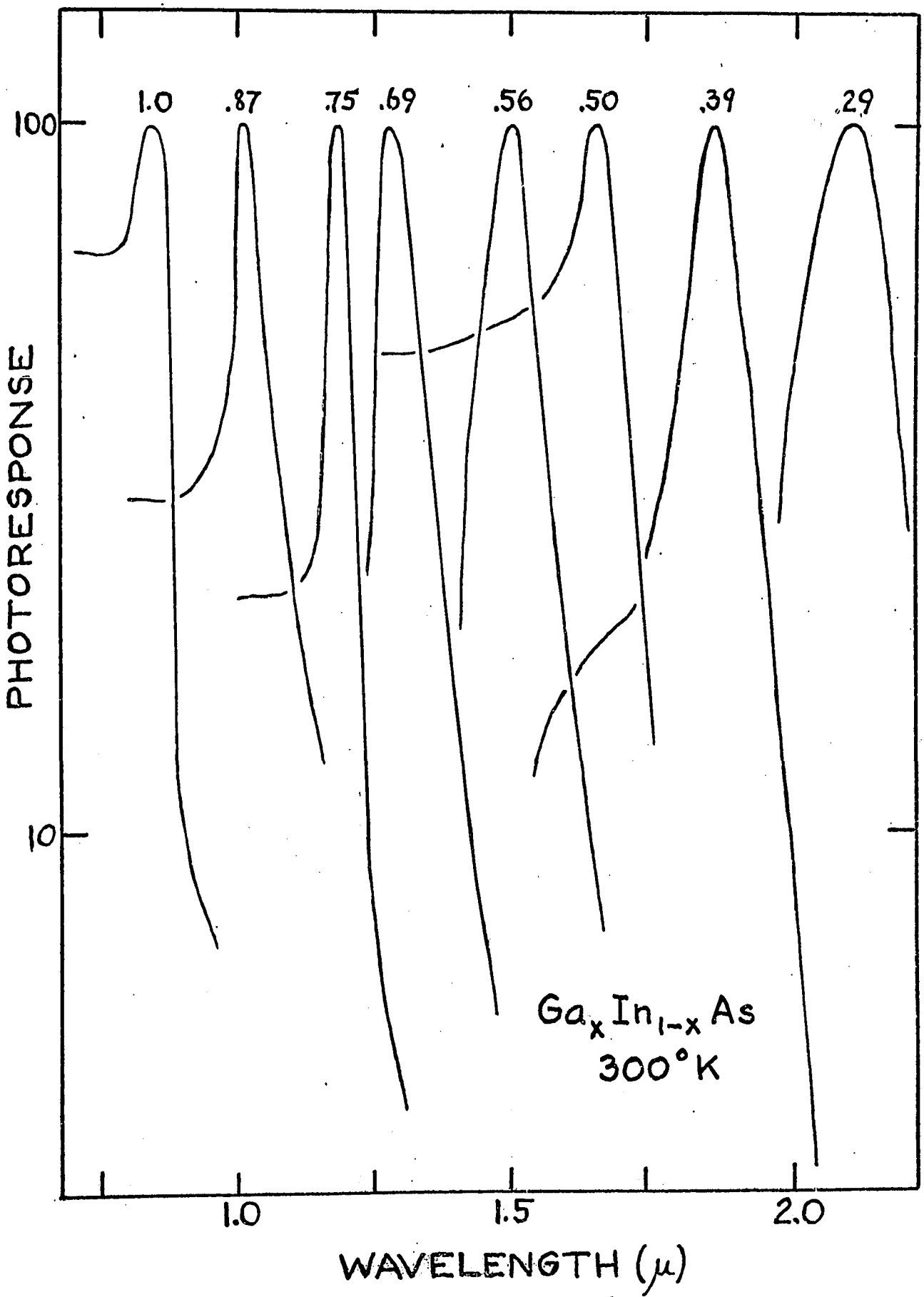

Fig. 19 PHOTORESPONSE CURVES FOR GaAs-InAs AT 300°K
Value for the mole fraction x is given above the curves

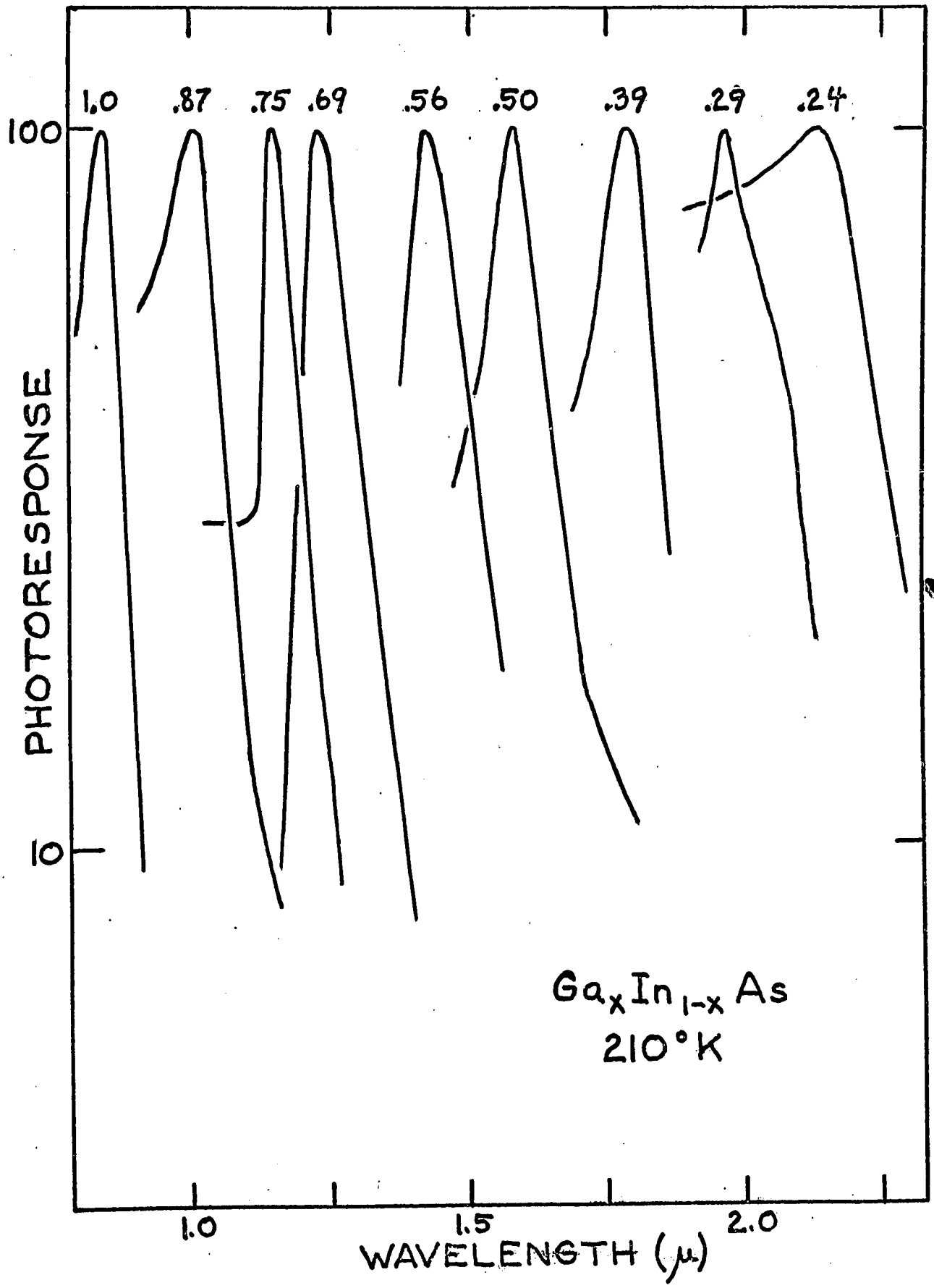

Fig. 20 PHOTORESPONSE CURVES FOR GaAs-InAs AT 210°K

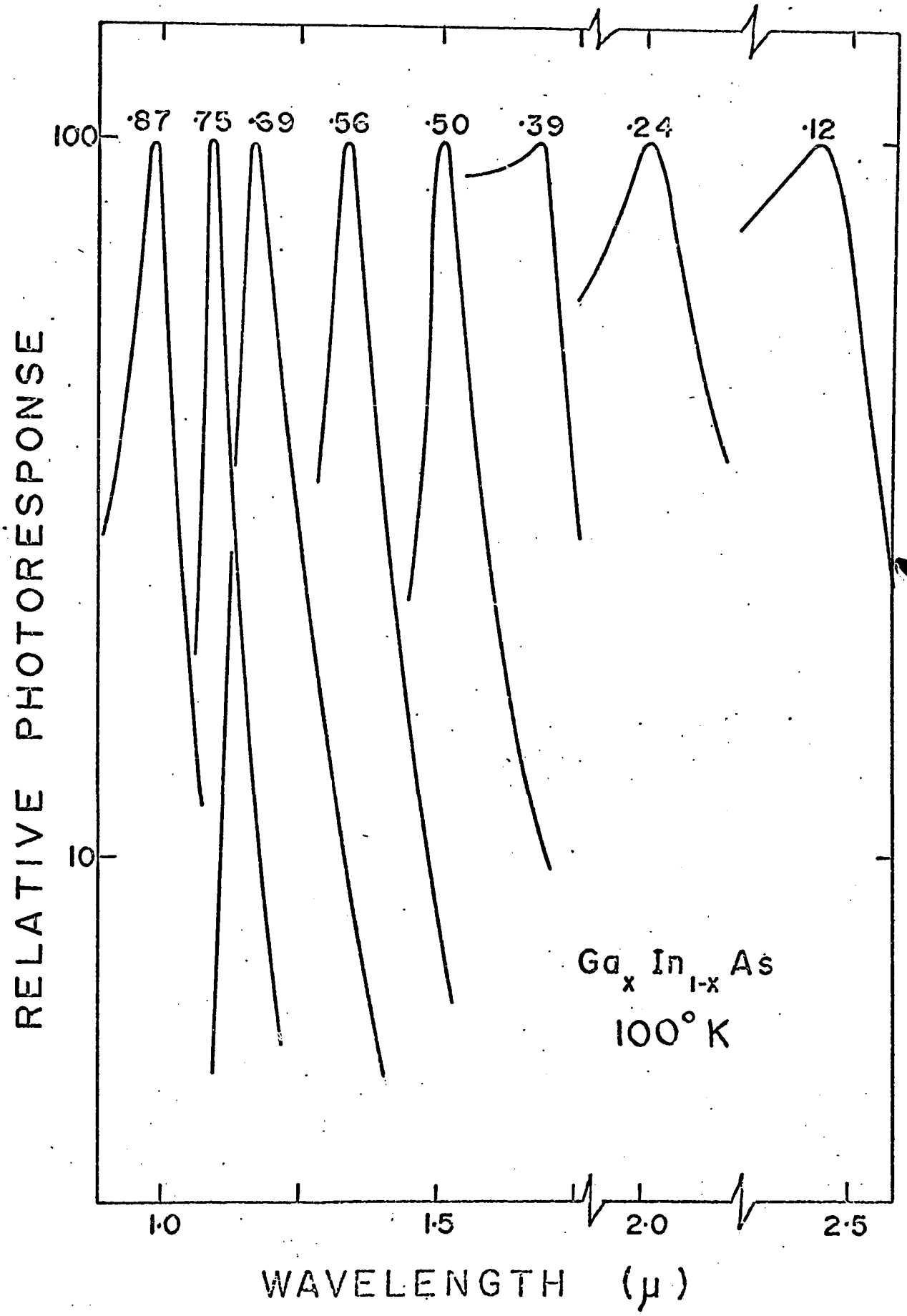

Fig. 21 PHOTORESPONSE CURVES FOR GaAs-InAs AT 100°K

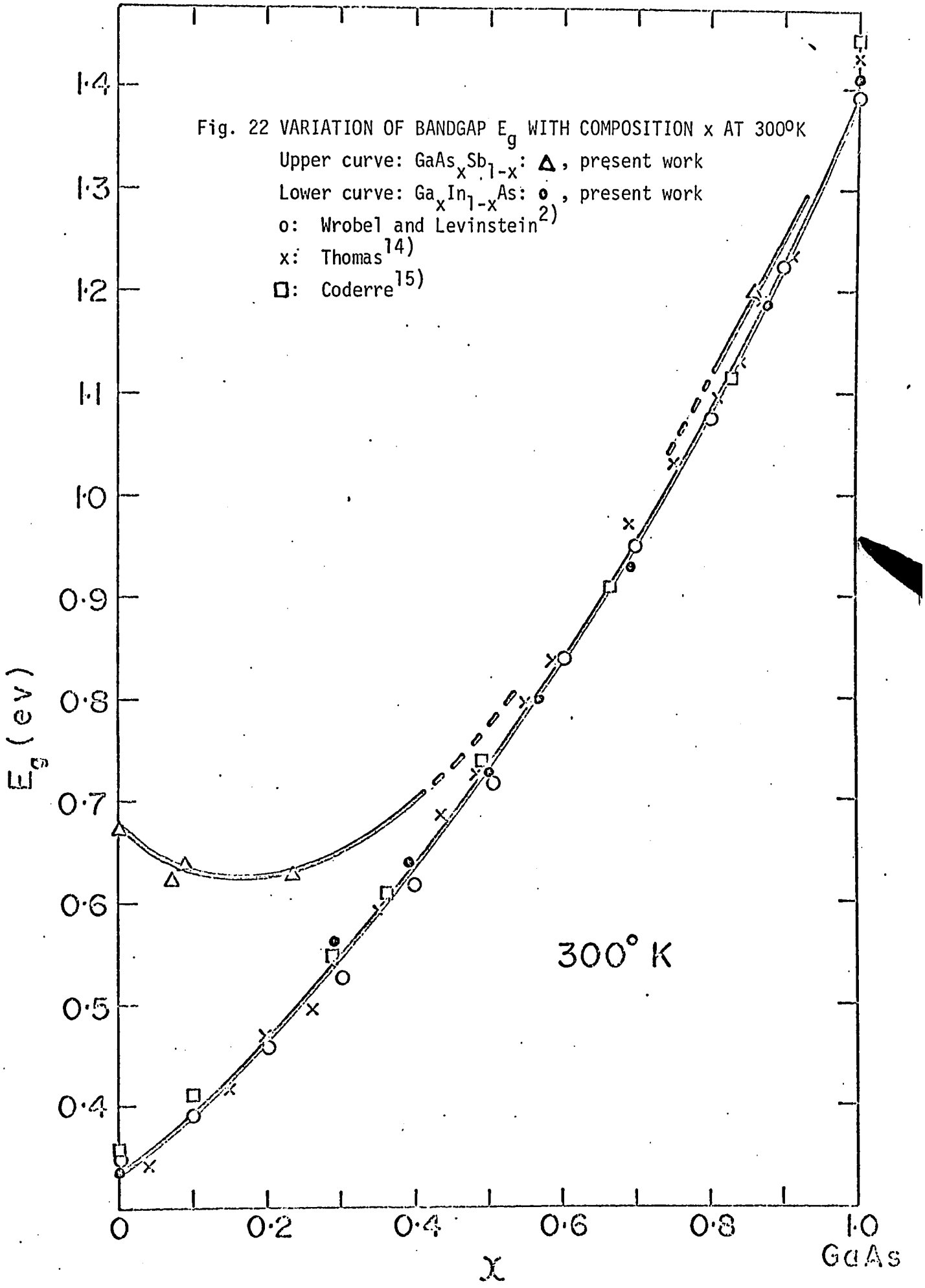

Fig. 22 VARIATION OF BANDGAP E_g WITH COMPOSITION x AT 300°K

Upper curve: $GaAs_xSb_{1-x}$: △, present work

Lower curve: $Ga_xIn_{1-x}As$: o, present work

o: Wrobel and Levinstein[2)]

x: Thomas[14)]

□: Coderre[15)]

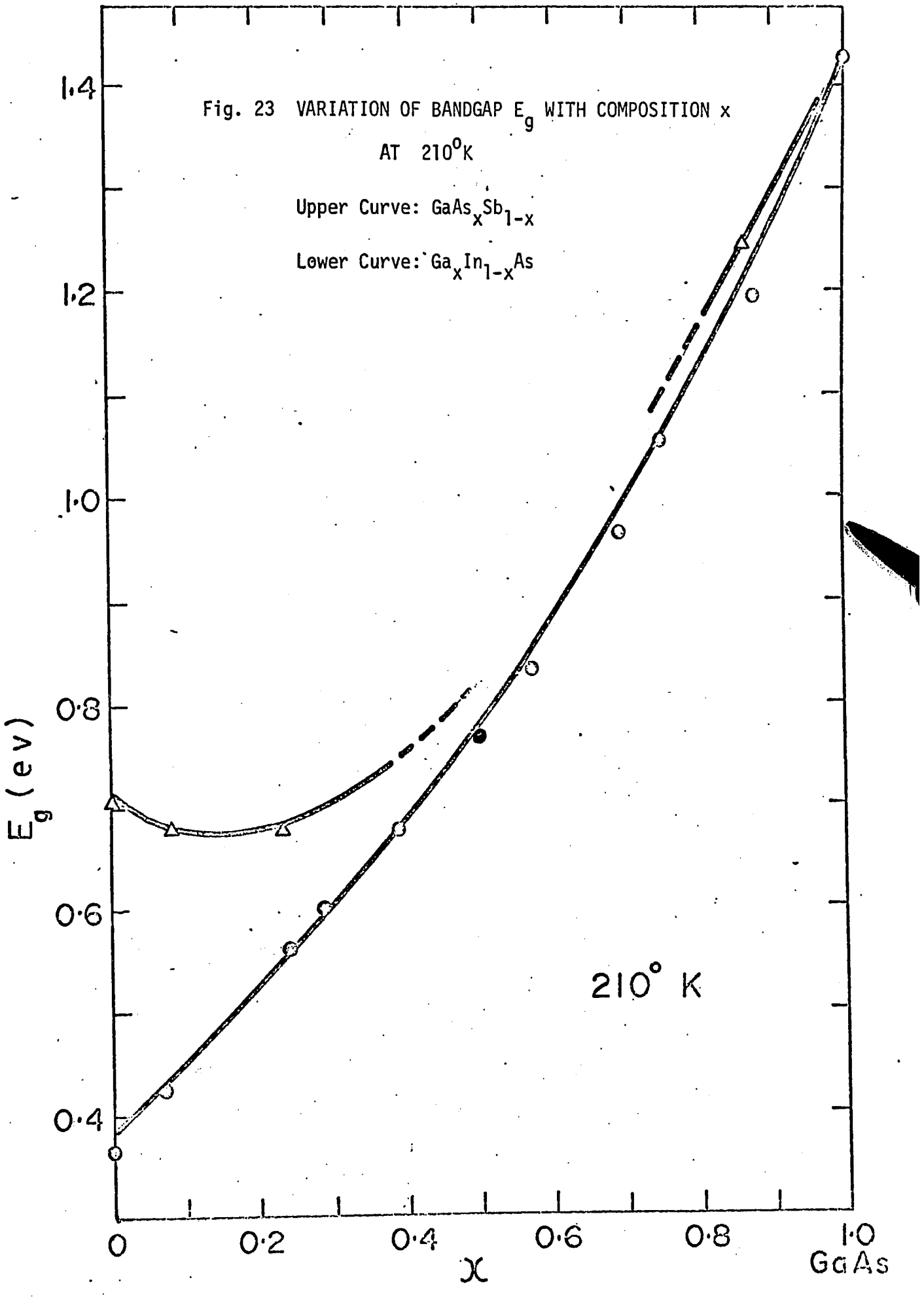

Fig. 23 VARIATION OF BANDGAP E_g WITH COMPOSITION x AT 210°K

Upper Curve: $GaAs_xSb_{1-x}$

Lower Curve: $Ga_xIn_{1-x}As$

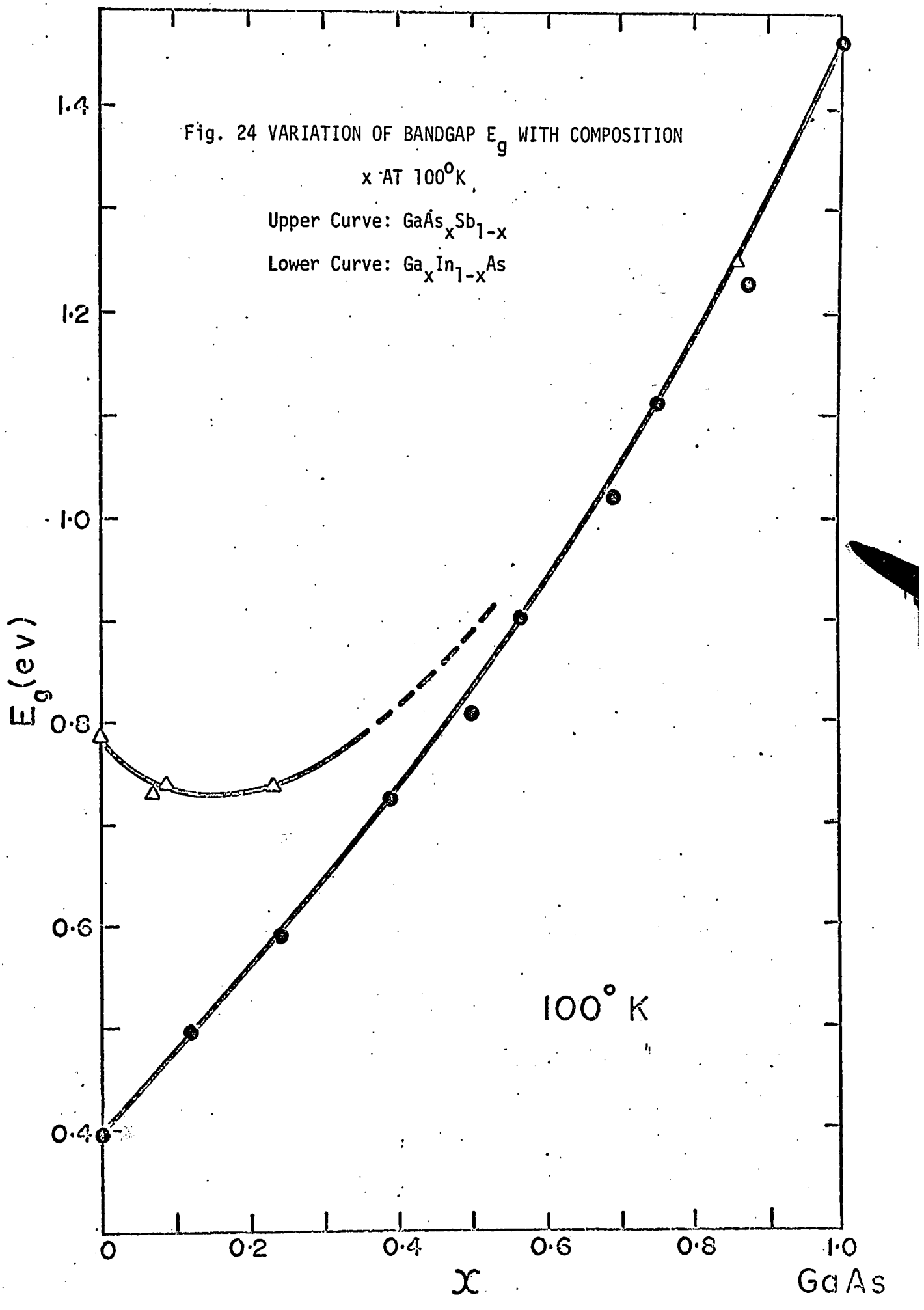

Fig. 24 VARIATION OF BANDGAP E_g WITH COMPOSITION x AT 100°K

Upper Curve: $GaAs_xSb_{1-x}$

Lower Curve: $Ga_xIn_{1-x}As$

measurements and these electrical results compare favourably with the optical values.

The scatter observed in the points of the present work is small enough to be considered experimental error. As mentioned in Chapter III.8 (iv) there is a small uncertainty in the composition. The bandgaps at lower temperatures show more scatter than at room temperature; this is believed to result largely from the temperature variation among runs. Thermocouple measurements showed a scatter of up to ± 10 degrees from the average values of 210°K and 100°K. Differences between the values of the present investigation and those of other workers could arise from the different criteria used to measure bandgaps.

IV.3 GaAs-GaSb

i) Ingots

To date, alloys across the entire composition range between GaAs and GaSb have not been produced. Homogeneous alloy material up to about 35 mole percent GaAs, and beyond 80 percent, were made in this laboratory by Thomas[16] who also determined the carrier concentrations. GaAs-rich samples were n-type with carrier concentrations of the order of 10^{16} cm^{-3} while the GaSb-rich samples were p-type of the order of 10^{17} cm^{-3}. Six samples were done in this system.

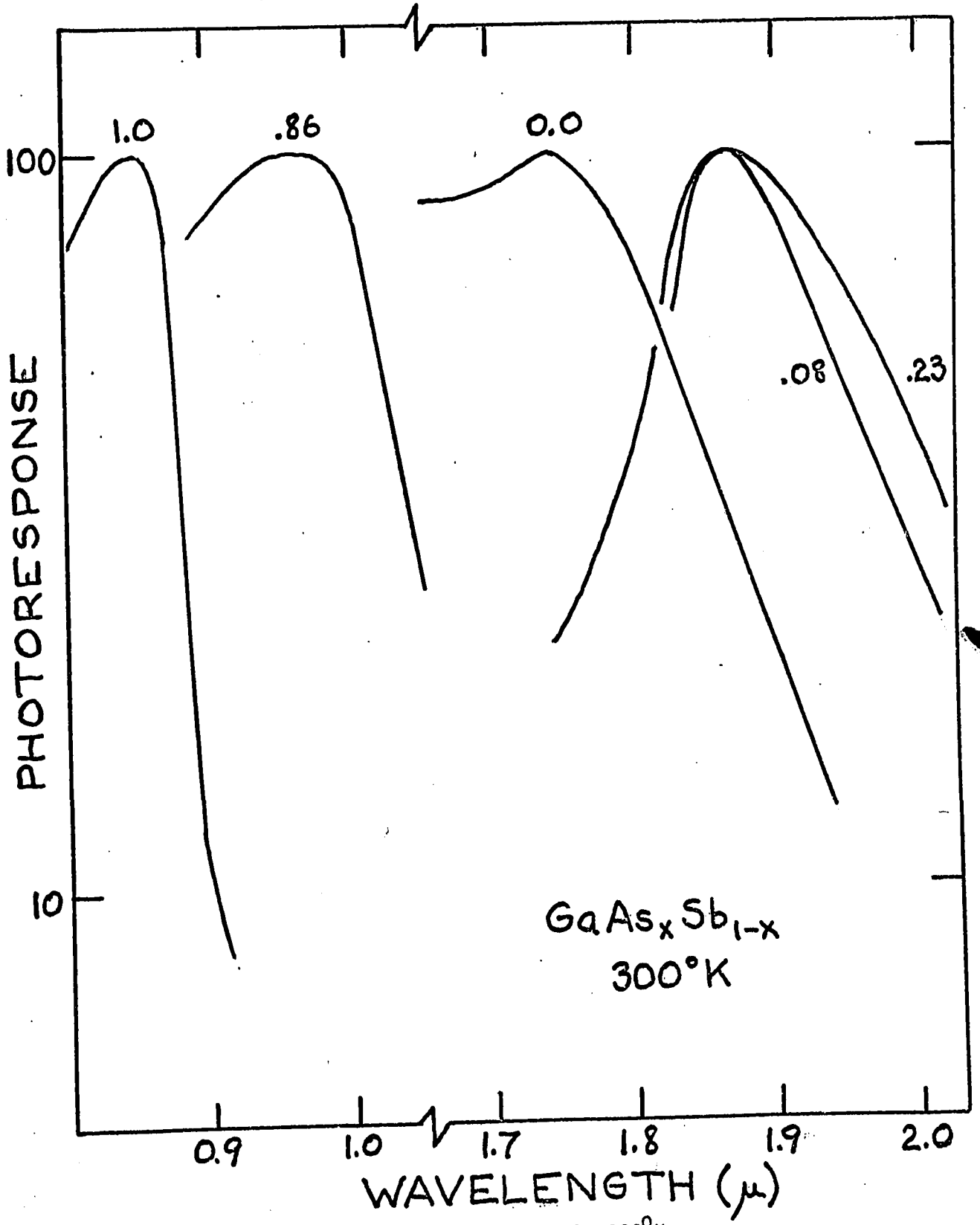

Fig. 25 PHOTORESPONSE CURVES FOR GaAs-GaSb AT 300°K
Value for the mole fraction x is given above the curves

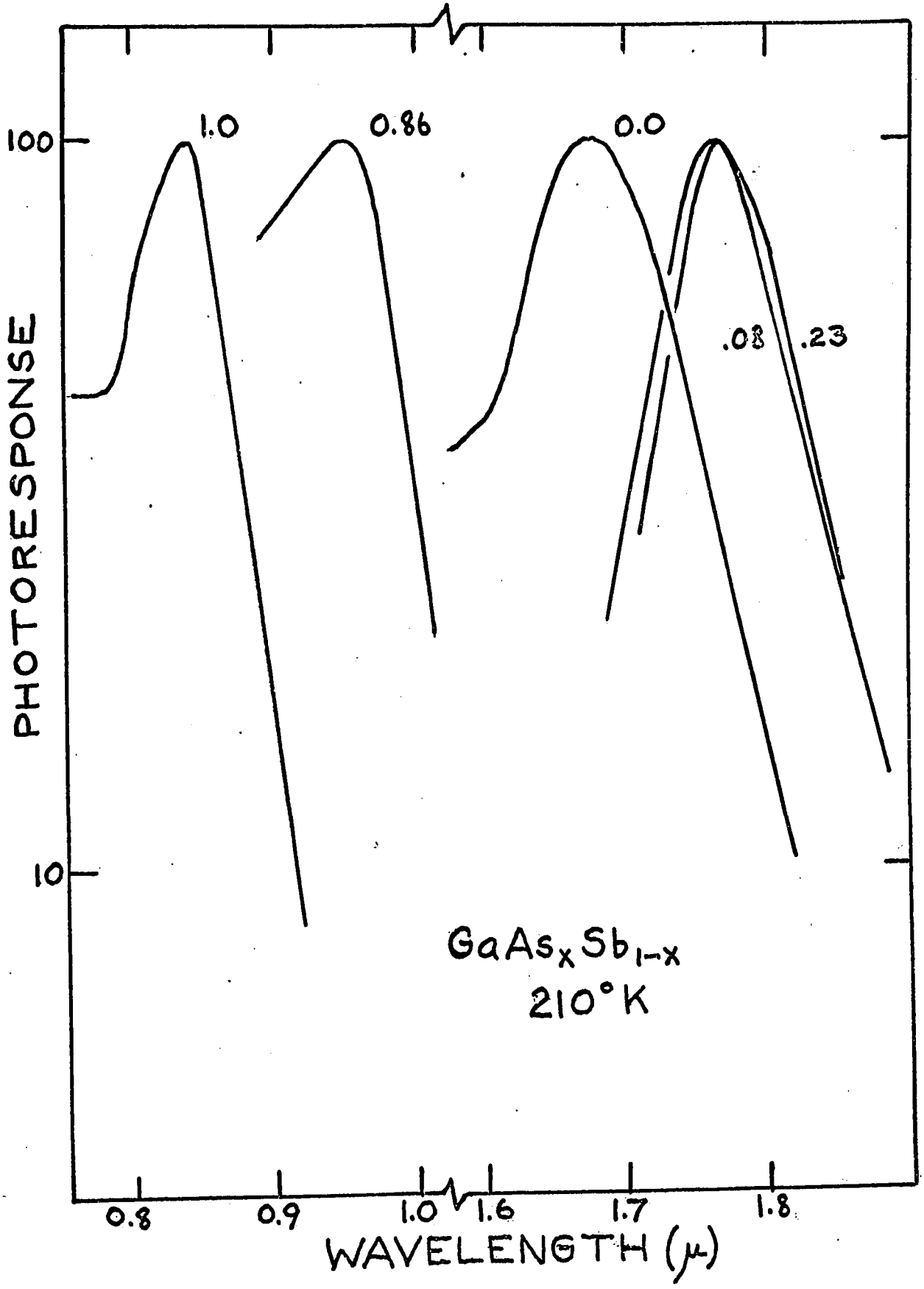

Fig. 26 PHOTORESPONSE CURVES FOR GaAs-GaSb AT 210°K

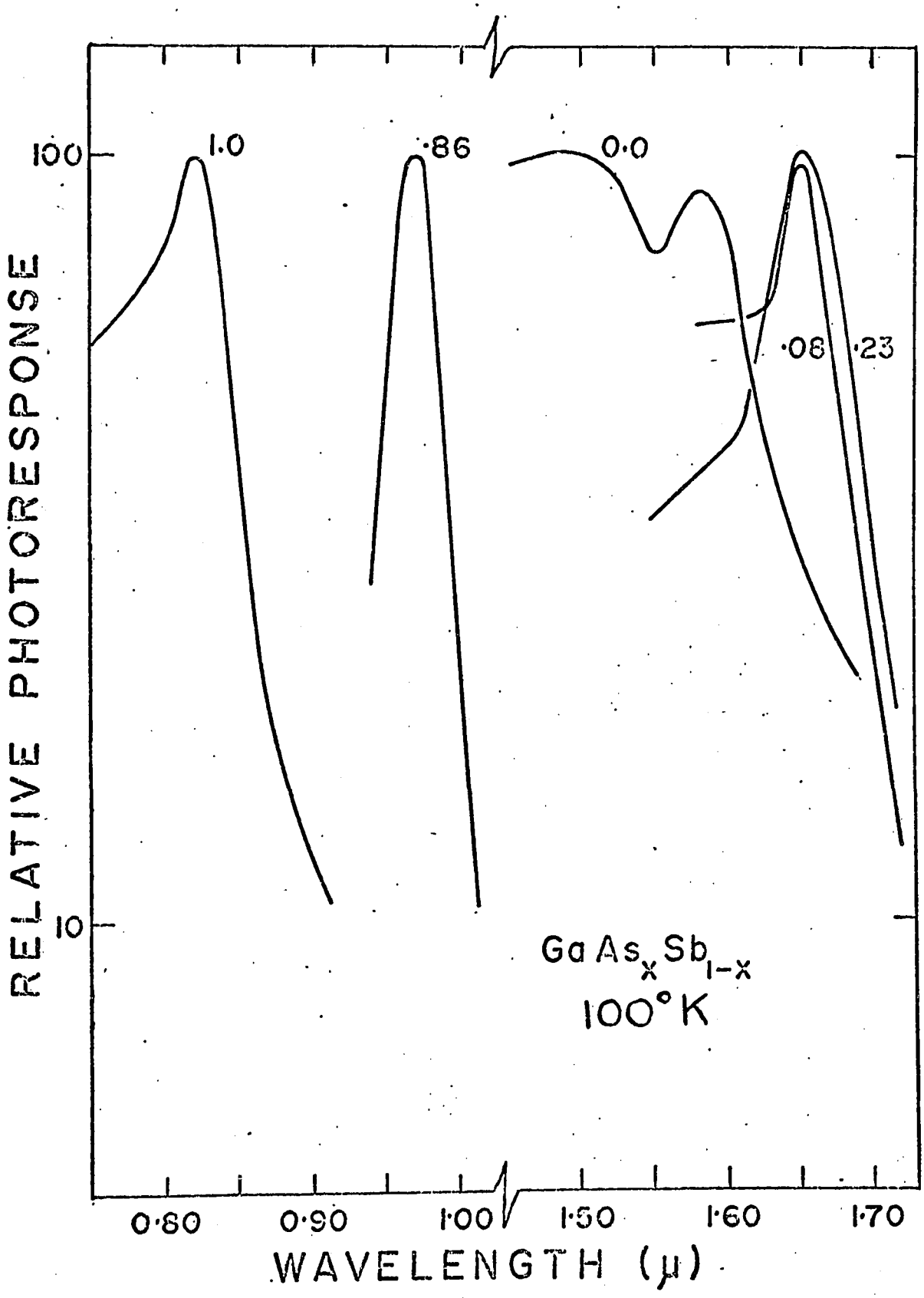

Fig. 27 PHOTORESPONSE CURVES FOR GaAs-GaSb AT 100°K

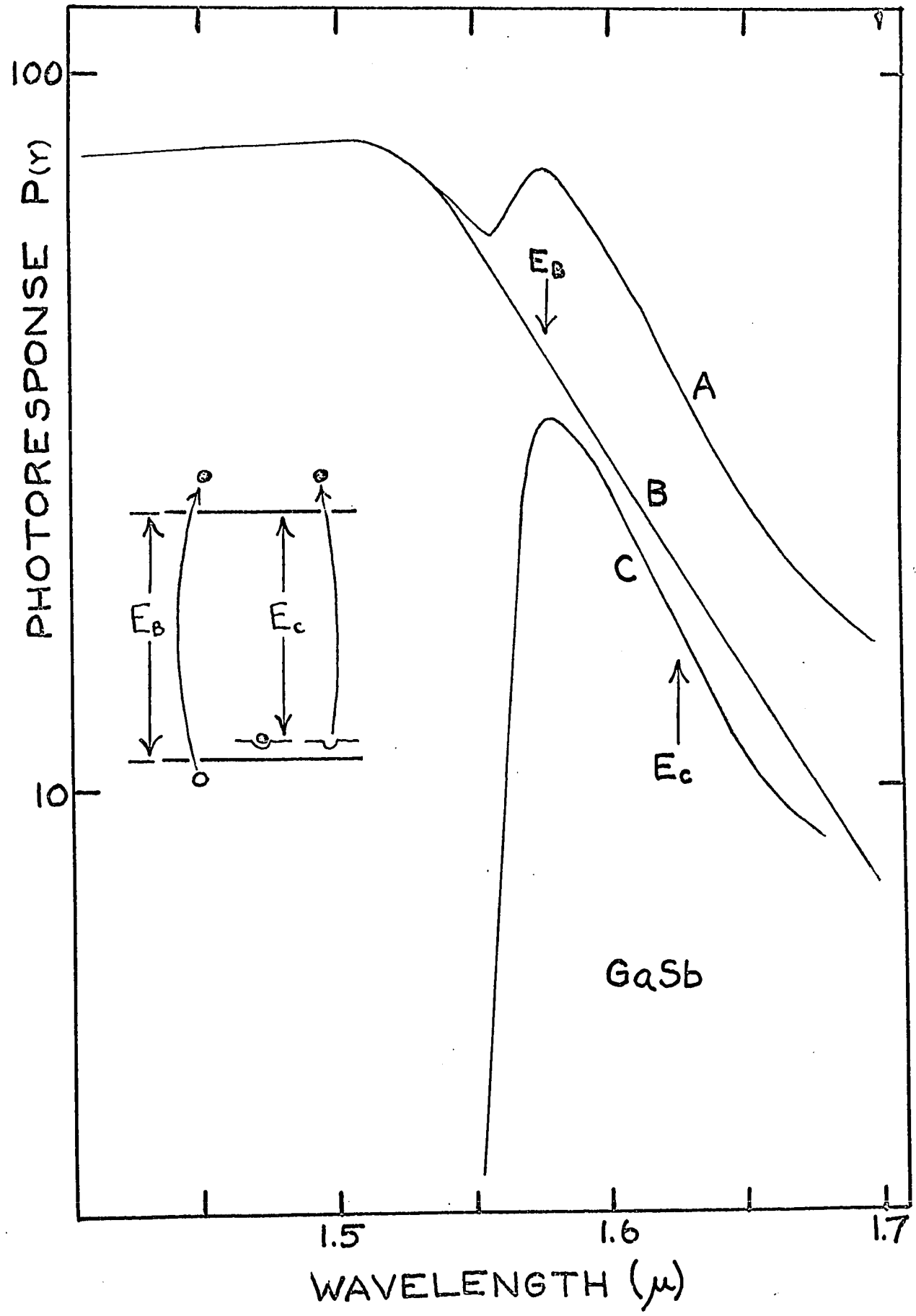

Fig. 28 PHOTORESPONSE FOR GaSb AT 100°K, UPPER CURVE A
Upper arrow: Bandgap for postulated intrinsic response B
Lower arrow: Bandgap for postulated impurity response C

ii) Photoresponse results

The graphs for this system are presented in a format similar to that used for GaAs-InAs. The curves in the lower part of figure 18 give the spectral response at three temperatures for $GaAs_{.23}Sb_{.77}$. With a bias of 1.4 volts, the peak signal at room temperature before amplification was 1×10^{-7} volts. Photoresponse curves for the remaining samples at these temperatures are given in figures 25, 26 and 27. Again, these curves show behaviour expected from theory, but a couple of points will be mentioned. Whereas for GaAs-InAs all the alloy responses fall between those of the end compounds, for GaAs-GaSb the curves for samples of composition $x = .08$ and $= .23$ lie at longer wavelengths than this range. This is immediate evidence for an energy minimum in the bandgap variation with composition, to be seen more explicitly later. Also, the photoresponse at $100^{o}K$ for GaSb shows a feature seen for no other samples in this work. The pronounced dip occurring near the absorption edge was postulated to arise from an imperfection level lying close to the valence band.

On the basis of this postulate, an attempt was made to separate this impurity photoconductivity from the intrinsic response, and thereby to estimate the energy level. The technique is shown in figure 28. Previous observation of spectral response curves assisted in extending the decay exponentially beyond the initial peak; the resulting curve "B" was assumed to be the intrinsic response with a bandgap of 0.788 ev.

Substracting the ordinates P(B) of this curve from those of the observed photoresponse "A" yields a third curve, "C". This is the response arising solely from the postulated imperfectipn; applying Moss' criterion (Chap. II.5) to curve "C" gives an imperfection activation energy of 0.763 ev, smaller than the intrinsic activation energy by 0.025 ev. A possible energy level scheme is shown with the imperfection level lying just above the valence band.

The investigations of other workers on GaSb have shown an energy level 0.034 ev above the valence band. Habegger and Fran[17] observed it in their photoconductivity results. Johnson[18] gives a survey of the observations of this level and others in GaSb. It is believed that this level arises from a lattice imperfection rather than an impurity atom.

An estimate of the concentration of such an imperfection can be made from the relative intensity of the intrinsic and imperfection responses. Wrobel and Levinstein[2] observed impurity responses in InAs and assumed that the photosignal from each is proportional to the number of those impurity centers. In the present case, the intrinsic photoresponse arises from a p-type carrier concentration of about 10^{17} cm^{-3}. The peak impurity photoresponse is about 40$ of the intrinsic response, and, on such

an assumption, results from a concentration of imperfections of approximately 4×10^{16} cm^{-3}.

Although the initial extrapolation of the intrinsic response is somewhat arbitrary, the above construction may indicate a possible origin for this unusual feature.

iii) Bandgap values

Despite the limited range of alloy material available, the bandgaps of the samples studied do suggest a probable parabolic variation with composition. This is shown explicitly in fig. 22 at room temperature, and in figures 23 and 24 at 210°K and 100°K. Of interest is the pronounced minimum in the bandgap variation near $x = 0.2$ at all three temperatures; this was observed previously by Thomas et al[16] in their room temperature absorption data. Incidentally, the variation of bandgap for InAs-InSb shows a similar behaviour[9].

iv) Bandgap values for the end compounds

Generally accepted values for optical bandgaps are available only for the compounds. Such values from this work are presented explicitly in Table II for ease of comparison with the accepted values[10]. Bandgaps obtained for individual samples of InAs are included, as mentioned earlier.

IV.4 GaSb-InSb

The several samples attempted in this system were taken from ingots prepared in this laboratory by Coderre[19] and had carrier concentrations of the order of 10^{17} cm^{-3}, being p-type near the GaSb end. Following the lack of results with InSb, a signal was not expected in this system for InSb-rich samples. However, with the assistance of Mr. A. Filion, several GaSb-rich samples were tried but only one at 88% GaSb was successful. The bandgaps obtained for it were 0.573 ev at room temperature, 0.592 ev at 210^{o}K, and 0.595 ev at 100^{o}K. Wrobel and Levinstein's[2] transmission results predict a value of 0.567 ev at room temperature for this composition. The cause of the unusual difficulty in this system is not known.

CHAPTER V

PERFORMANCE AS DETECTORS

V.I Motivation

On studying the photoresponse curves presented in the previous chapter, a couple of features which would be of considerable use in applications are apparent. First, a sample may be chosen with a photoresponse threshold anywhere over a range of infrared wavelengths. For the III-V compounds, thresholds are available up to 6 microns; for the alloys studied in this investigation, the bandgaps lie between 0.8 microns and 3.5 microns. Figures 19, 20 and 21 for GaAs-InAs, and 25, 26 and 27 for GaAs-GaSb illustrate this spread of photoresponse across the alloy range. They show as well that a response is obtainable at room temperature or lower. Second, for a chosen threshold, the width of the curve and its short wavelength response can be varied somewhat by surface treatment. It may be recalled that at wavelengths shorter than the spectral peak, the absorption constant is high, and the photocarriers are created near the surface. Milner-Brown[13], in work done in this laboratory, has shown the effect of surface treatment on GaAs is to vary the lifetimes of these carriers.

In addition, he illustrated the possibility of using a transverse magnetic field to deflect the surface carriers into the volume of the sample, and hence increasing their lifetime. This has the effect of raising, of flattening, the spectral sensitivity at shorter wavelengths.

The potential of these materials as detectors is apparent; however, their performance relative to existing infrared detectors must be considered. Such comparison can be made most easily through detector parameters which largely eliminate the dependence of the response on illumination intensity, surface area, signal to noise ratio and the electronic system used. Many parameters have been in use over the years; some are more useful than others and only several are in frequent use. R.D. Hudson[20], in "Infrared Systems Engineering", outlines some of these.

V.2 Parameters describing detector performance

Responsivity is defined as the detector output voltage per unit irradiance and unit active area.

$$R = \frac{V_s}{HA_d} \quad \text{volts(watt)}^{-1} \qquad (5\text{-}1)$$

where V = signal voltage at the detector (volts rms)

H = rms irradiance (watt cm^{-2})

A_d = active detector area (cm^2)

Responsivity measurements should be accompanied by a quotation of some of the conditions of the measuring system, like bias, temperature, and electronics used.

However, the responsivity gives no indication of the minimum radiant flux that can be detected, since it does not include the amount of noise which may ultimately obscure the signal. A parameter which includes the signal to noise ratio rather than the signal voltage alone is the noise equivalent power NEP, defined as the radiant flux necessary to give an output signal equal to the detector noise.

$$NEP = \frac{H A_d V_n}{V_s} \quad \text{watts} \qquad (5\text{-}2)$$

where V_n = rms noise at the detector output. Presumably, the lower the NEP the better the detector. A more convenient parameter would be the inverse of NEP,

$$D = \frac{1}{NEP} \quad (\text{watt})^{-1} \qquad (5\text{-}3)$$

There is no simple theoretical relationship between D and conditions of measurement such as wavelength, detector temperature, chopping frequency, and bias. However, extensive theoretical and experimental studies have shown that the dependence of D on surface area and the bandwidth of the electronics is approximately[20]

$$D\,(A_d\ \Delta f)^{\frac{1}{2}} = \text{constant} \qquad (5\text{-}4)$$

where Δf = equivalent noise bandwidth of the associated electronics. As this constant contains as many of the variables as may be readily included, it is one of the more popular detector parameters; it is called the detectivity, D*. Thus,

$$D^* = D\,(A_d\ \Delta f)^{\frac{1}{2}} = \frac{(\Delta f)^{\frac{1}{2}}\, V_s}{H\, A_d^{\frac{1}{2}}\, V_n}\ \text{cm}(\text{Hz})^{\frac{1}{2}}\ (\text{watt})^{-1} \qquad (5\text{-}5)$$

The conditions of measurement usually quoted with D* are blackbody temperature (or source power), wavelength, chopping frequency, and detector temperature.

V.3 Results for samples in this work

Preliminary measurements of R and D* were done on the same samples as used above, and under the same experimental conditions.

They yield room temperature responsivity values generally in the range $10^{-3} < R < 10^{-2}$ volts(watt)$^{-1}$. As a comparison, a similar measurement on an evaporated PbSe cell (Kodak Type E Ektron Detector) yields a value for R of 50 volts(watt)$^{-1}$. The room temperature detectivity values lie in the range $5 \times 10^{-4} < D^* < 8 \times 10^{6}$ cm(Hz)$^{\frac{1}{2}}$(watt)$^{-1}$ compared with 4×10^{8} for the PbSe cell. At 100^{o}K the detectivity values are about an order of magnitude larger.

A summary of D* values is given in Table III. There is some scatter among the values but a trend can be noted. The D* figures for GaAs-rich samples are generally larger than for GaSb and InAs-rich samples. In this regard, it is interesting to note that for the experimental work described in Chapter IV, response curves were obtained more readily for GaAs-rich specimens than for GaSb and InAs.

D* is a characteristic of a particular sample as well as a particular material. For a given irradiance, bandwidth and sample area, the detectivity is influenced largely by surface treatment, sample dimensions and the carrier concentration. The variation of the surface preparation from one sample to another is believed to be the cause of the scatter among the results for each system.

TABLE III : ROOM TEMPERATURE VALUES OF D* MEASURED AT PEAK WAVELENGTH (λ_m)

$Ga_xIn_{1-x}As$	λ_m	D*
x	microns	$cm(Hz)^{\frac{1}{2}}(watt)^{-1}$
0	3.5	1.9×10^5
.29	2.1	5.6×10^4
.39	1.87	2.8×10^5
.50	1.6	7.4×10^5
.56	1.5	2.1×10^5
.69	1.3	2.1×10^5
.75	1.2	8.4×10^6
1.00	0.87	2.4×10^6
$GaAs_xSb_{1-x}$		
0	1.75	5.4×10^5
.08	1.87	5.8×10^5
.23	1.87	2.2×10^5
.86	1.0	1.6×10^6
PbSe (Kodak)	3.5	4.1×10^8

Such preliminary results are encouraging. Hopefully further study into sample preparation would improve the D* figures and allow the III-V alloys to compete successfully with existing quantum detector.

CHAPTER VI

CONCLUSION

There were three goals in this work:

1) to set up a monochromator system and low signal detection electronics that would be useful in photoconductivity and a variety of similar experiments in the infrared;

2) to perform basic photoconductive studies of the III-V alloys to complement the extensive optical and electrical studies undertaken on these in this laboratory, and

3) to make a preliminary assessment of the potential of some of these alloys as infrared detectors.

The optics and light source layout designed by the author to accompany the monochromator have proven satisfactory in this work, and versatile in other experiments performed on this equipment as well. The low level signal detection system, consisting principally of a low noise preamplifier and a lock-in amplifier, has been used in this work to recover photosignals as low as 2×10^{-8} volts with an excellent signal to noise ratio, from samples having resistances of a couple of ohms. This is close to the design limit of electronics.

Using 'as grown' alloys with carrier concentrations in the range 10^{16} to 10^{18} cm^{-3}, good results were obtained for the photo-response from two alloy systems. Twelve samples of GaAs-InAs, done at $300^{o}K$, $210^{o}K$ and $100^{o}K$ gave a spread of response curves across the alloy range. Moss' criterion was used to determine the bandgaps. A smooth variation of optical energy gap with composition resulted at the three temperatures; previous work done by other investigators at room temperature showed close agreement and indicated the degree of success of the techniques used here. Similar results were obtained for the GaAs-GaSb system. The complete alloy range is not yet available, and little work has been done on the bandgap variation. However, responses of the six samples taken from near the ends of the alloy range suggest a minimum in a smooth variation of bandgap with composition at the three temperatures.

Finally, the preliminary figures on the performance of these alloys as detector material were encouraging. While their responsivity and detectivity values were somewhat low, further study of sample preparation, and perhaps of suitable compensation at time of growth, may improve these. The possibility of making from these alloys infrared detectors with thresholds anywhere in the range from 0.8 to 3.5 microns justifies further applied studies being undertaken.

LIST OF REFERENCES

1. Smith, W. Nature 7 303 (1873)
2. Wrobel, J. S. and Levinstein, H. Infrared Physics 7, 201 (1967)
3. Smith, R. A. Semiconductors (Cambridge), p. 303-312 (1964)
4. Moss, T. S. Photoconductivity in the Elements (Butterworths), p. 30-34 (1952)
5. Madelung, O. Physics of III-V Compounds (Wiley), p. 18 (1964)
6. Dekker, A. J. Solid State Physics (Prentice-Hall), p. 366 (1963)
7. Ramsey, W. Y. and Alishouse, J. C. Infrared Physics 8 143 (1968)
8. Madelung, O. p. 272
9. Coderre, W. M. and Woolley, J. C. Can. J. Phys. 46, 1207 (1968)
10. Long, D. Energy Bands in Semiconductors (Wiley), p. 111 (1968)
11. Thomas, M. B. Ph.D. Thesis, University of Ottawa, p. 53 (1969)
12. Coderre, W. M. Ph.D. Thesis, University of Ottawa, p. 72 (1969)
13. Milner-Brown, H. and Fortin, E. Can. J. Phys. 47, 2789 (1969)
14. Thomas, M. B. Ph.D. Thesis, p. 120
15. Coderre, W. M. Ph.D. Thesis, p. 234
16. Thomas, M. B., Coderre, W. M. and Woolley, J. C. Submitted for publication to the Can. J. Phys. (1970)
17. Habegger, M. A. and Fan, H. Y. Phys. Rev. 138 A598 (1965)
18. Johnson, E. J. in Optical Properties of III-V Compounds, R. K. Willardson and A. C. Berr, ed. (Academic Press), p. 205 (1967)

19. Coderre, W. M. Ph.D. Thesis, p. 65

20. Hudson, R. D. Infrared Systems Engineering (Wiley), chapter 7 (1970)

21. Moss, T. S. Optical Properties of Semiconductors (Butterworths), p. 63 (1959).